

THE EFFECT OF SILICON OXIDE ADDITIVE ON THE PROPERTIES OF HYDROXYAPATITE-1 WT. % MAGNESIUM OXIDE BINARY COMPOSITE

#SULEYMAN SERDAR PAZARLIOGLU*, OGULCAN ALGAN**

*Marmara University, Technology Faculty, The Department of Metallurgy and Materials Engineering, Recep Tayyip Erdogan Campus, 34854, Maltepe, Istanbul, Turkey

**Marmara University, Institute of Pure and Applied Sciences, Goztepe Campus, Istanbul, Turkey

#E-mail: spazarlioglu@marmara.edu.tr

Submitted August 9, 2023; accepted September 15, 2023

Keywords: Hydroxyapatite, Magnesium Oxide, Silicon Oxide, Sintering

A hydroxyapatite-1 wt. % magnesium oxide (HA-1M) composite with and without a silicon oxide (SiO₂) additive at amounts of 0.25, 0.5, and 1.0 wt. % was sintered between 1100 and 1300 °C to investigate the effect of the SiO₂ additive on the sintering behaviour, mechanical properties and in vitro bioactivity of HA-1M. The HA-1M composite consists of HA, whitlockite and farringtonite. In the SiO₂ added samples, the phases of akermanite, clinopyroxene, merwinite, melilite and diopside were detected. These phases contributed to achieving better mechanical properties in the SiO₂ added samples than that of the HA-1M composite. The highest fracture toughness ($1.47 \pm 0.04 \text{ MPa}\cdot\text{m}^{1/2}$) and compression strength ($183 \pm 25.09 \text{ MPa}$) were achieved by sintering the HA-1M composite at 1200 °C. In the SiO₂ added samples, the highest compression strength and fracture toughness were calculated as $201.53 \pm 18.01 \text{ MPa}$ and $1.78 \pm 0.22 \text{ MPa}\cdot\text{m}^{1/2}$, respectively, which belongs to the HA-1M-0.5SiO₂ composite. With the addition of SiO₂ at an amount of 0.5 wt. %, the ratio of the apatite layer formed on the surface of the HA-1M composite increased.

INTRODUCTION

The availability of innovative bioceramics able to stimulate the repair of biological tissues, in particular for the treatment of bone defects, represents a current need in medicine [1]. Hydroxyapatite (HA) is an important mineral making the hard component of tissues, such as bones, teeth, and tendons that gives these organs stability, strength and improves their mechanical and chemical performance [2]. It also possesses excellent biocompatibility and osteogenic properties [3]. These attractive properties have encouraged its production by various methods, including biological [4], chemical [5] methods and in commercial purity [6]. However; since none of them have sufficient mechanical strength, they cannot be used in applications requiring a load-bearing capacity in the human body. The properties of HA can be modified by dopant and/or substitution materials. Various substitutions, such as fluorine [7], zinc [8], copper [9], strontium [10], have been used to improve the properties of HA. Magnesium (Mg) has also used as a substitute in HA [11]. It is closely associated with the mineralisation of calcified tissues, directly stimulating

osteoblast proliferation. Mg depletion adversely affects all stages of skeletal metabolism, causing the cessation of bone growth, decreased osteoblastic and osteoclastic activities, osteopenia and bone fragility [12]. The ultra-low elastic modulus (45 GPa) of this element (close to bone tissue (2-20 GPa)) minimises the problems caused by stress shielding. This material also has an ultra-low density ($1.74 \text{ g}\cdot\text{cm}^3$), an excellent tissue healing rate, a high strength-to-weight ratio, and a low cost. Despite all these advantages, the low corrosion resistance of Mg in physiological environments has limited its incorporation with HA [13]. One way to overcome that problem noted for Mg is to use an Mg-containing compound such as magnesium oxide (MgO) [14]. It has been extensively used for many years as an orthopaedic implant material that exhibits excellent biocompatibility and high mechanical strength [15]. It is biocompatible and non-toxic; and can be a viable dispersing phase to produce a biocomposite. On the other hand, MgO degrades slowly compared with pure Mg [16]. Existing studies in the literature have revealed that MgO both increases the properties of HA and enhances the ability of osteoinduction and osteogenesis in the bone repair

[17]. While previous studies have attempted to improve the poor mechanical properties of HA with the addition of different proportions of MgO, none of them reported a significant increase in the mechanical properties. The highest compression strengths of 55.6 MPa for [18], 116 MPa [19], 121.81 ± 7.0 MPa [20] were reported to HA-MgO composites, whilst the addition of 1 wt. % MgO to HA showed the best sintering performance. Tan et al., were able to obtain a fracture toughness of 1.48 ± 0.17 MPa·m^{1/2} for 1.0 wt. % MgO added HA [21]. If the MgO addition is more than 1 wt. %, it also causes an increase in the decomposition rate of HA. For example, Evis et al., reported that the addition of 5 wt. % MgO causes 80 % thermal decomposition in the HA-40 % ZrO₂ binary system [22]. In order to improve the properties of the HA-1 wt. % MgO composite, several studies have been carried out in which materials, such as niobium oxide (Nb₂O₅), strontium oxide (SrO) and lanthanum oxide (La₂O₃), have been added. The following results are reported from these studies: The addition of 1 wt. % SrO to an HA-1 wt. % MgO composite was reported to cause decomposition of 66.27 % of HA to β-TCP, 7.83 % of HA to α-TCP and 6.02 % of HA to CaO [23]. A maximum compression strength of 96 ± 0.05 MPa was reported to an Nb₂O₅ added HA-MgO composite [24]. The addition of 1 wt. % La₂O₃ to an HA-1 wt. % MgO composite increased the compressive strength from 183.2 to 202.0 MPa, the fracture toughness from 1.37 to 2.32 MPa·m^{1/2} and decreased the brittleness index from 3.24 to 2.18 μm^{-1/2} [25].

Silicon (Si) is also an important element for the human body as it influences bone formation and calcification. Si has been reported to stimulate cellular activities, such as the proliferation and differentiation of osteoblast-like cells, mineralisation of human osteoblasts and osteogenic differentiation of mesenchymal stem cells. The importance of Si for bone formation has been demonstrated by indicating the presence of up to 0.5 wt. % Si in the osteoid of the bones of young mice and rats [26]. Moreover, Si substituted HA is also able to continuously supply ions which are essential for the process of bone reconstruction and biological processes [27]. However, it has been reported that the substitution of Si to HA causes the conversion of HA to the alpha-TCP phase, which has lower mechanical properties and a dissolution rate that is approximately 12 times higher than that of HA [28]. Moreover, the substitution of Si to HA also causes an increase in the number of dislocations and separation of grain boundaries from each other. It negatively affects its use in applications in the human body [29]. It has been stated that these problems can be overcome by doping HA with silica (SiO₂) instead of Si substitution [30]. Several studies have been undertaken to explain the effect of adding SiO₂ on the sintering behaviour of HA. HA with an SiO₂ addition results in the formation of calcium silicates that contribute to increasing the bioactivity of HA [31]. If the SiO₂ content

in HA is more than 1.5 wt. %, the HA-SiO₂ composite consists of pores, amorphous SiO₂ grains, unsintered regions and the transformation of HA into α-TCP, and leads to decrease in the sinterability of HA [32]. The addition of SiO₂ to a bovine HA-ZrO₂ composite was reported that its presence contributed to increasing the strength from 101 to 118 MPa [33]. Therefore, the idea has emerged that incorporating the advantages of both materials into HA could turn it into a suitable bone implant material. For that, SiO₂ between 0.25 wt. % and 1.0 wt. % was added to the HA-1 wt. % MgO composite and the effect of the SiO₂ addition on the properties of HA-1 wt. % MgO was investigated by a series of tests and material characterisation techniques.

EXPERIMENTAL

Hydroxyapatite (irregular form with an average grain size of 7.10 μm, Across Organics; Belgium), MgO (spherical form with an average grain size of 3.27 μm, 99.5 % in purity; Sigma Aldrich, USA), and SiO₂ (spherical form with an average grain size of 4.01 μm, 99.5 % in purity; Sigma Aldrich, USA) powders were mixed to prepare the composites as shown in Table 1. The composites were wet homogenised with the addition of ethyl alcohol and zirconia balls at 180 rpm for 2 h in a ball milling device, and then dried in an oven at 105 °C for 24 h. After drying, the green bodies were pelleted at 350 MPa at 11 ± 0.2 mm in height and length in accordance with our previous study [34]. They were sintered in air at 1100, 1200 and 1300 °C with a ramp rate of 5 °C·min⁻¹ over 4 h, and then cooled to room temperature at the same rate.

Table 1. Composition of the samples.

Sample ID	HA (wt. %)	MgO (wt. %)	SiO ₂ (wt. %)
HA	100	-	-
HA-1M	99	1.0	-
HA-1M-0.25S	98.75	1.0	0.25
HA-1M-0.5S	98.50	1.0	0.50
HA-1M-1S	98	1.0	1.0

After the sintering treatment, the properties of the sintered samples were determined by the measuring the shrinkage, density, porosity, relative density, hardness, fracture toughness, brittleness index and performing a compression test. The shrinkage in the samples were calculated using Equation 1.

$$S = \left(\frac{l_0 - l}{l_0} \right) \times 100 \quad (1)$$

Where *S*: Shrinkage, *l*₀: Length of the sample before sintering (mm), *l*: Length of the sample after sintering (mm).

The density and porosity of the samples were calculated by the Archimedes method using Equation 2 and 3, respectively. The relative density of the samples was calculated using Equation 4.

$$D = \left(\frac{w_d}{w_w - w_s} \right) \quad (2)$$

$$p = \left(\frac{w_w - w_d}{w_w - w_s} \right) \times 100 \quad (3)$$

Where D is the density ($\text{g}\cdot\text{cm}^{-3}$), w_d is the dry weight of the sample (g), w_w is the wet weight of the sample (g), and w_s is the wet weight of the sample in distilled water (g).

$$R_D = \left(\frac{D}{D_t} \right) \times 100 \quad (4)$$

Where R_D is the relative density (%), D_t is the theoretical density of the samples ($\text{g}\cdot\text{cm}^{-3}$) calculated by the mixture rule and taken as $3.156 \text{ g}\cdot\text{cm}^{-3}$ for HA [35], $3.58 \text{ g}\cdot\text{cm}^{-3}$ for MgO [36], and $2.20 \text{ g}\cdot\text{cm}^{-3}$ for SiO_2 [37].

The hardness of the samples was measured by a Future Tech FM 301 microhardness tester using an application load of 1.962 N at a dwell time of 20 s as it provided the formation of a hardness indent without cracking. It was calculated using Equation 5.

$$H_v = \frac{0.891x^F}{d^F} \quad (5)$$

Where H_v is the hardness, d is the average of the two diagonals of the imprint (mm), and F is the applied load (N).

The fracture toughness of the samples was determined on 1 μm polished samples using 2.943N loads for 10 s, according to Equation 6.

$$K_{IC} = 0.203 \left(\frac{c}{a} \right)^{-3/2} H_v \cdot a^{1/2} \quad (6)$$

Where; K_{IC} is the fracture toughness ($\text{MPa}\cdot\text{m}^{1/2}$), c is the radial crack dimension measured from the centre of the indent impression (m), and a is the half diagonal of the indentation (m).

The compressive strength of the samples was determined at a loading rate of 2 mm/min using a universal testing machine (Devotrans FU 50 kN, Turkey). Equation 7 was employed to calculate the brittleness index [38] of the samples, where B is the brittleness index, H_v is the hardness, and K_{IC} is the fracture toughness.

$$B = \frac{H_v}{K_{IC}} \quad (7)$$

The phases in the samples were analysed by a Philips X'Pert X-ray diffraction machine using $\text{Cu-K}\alpha$ as the radiation source at a scan speed of 0.6° per minute and a step scan of 0.02° in the range of 2θ values between 25° and 50° . The percentage of the phases

was determined by Rietveld analysis. The surface morphology of the samples were determined by an FEI Sirion XL30 Scanning Electron Microscope (SEM) machine. The average grain size of the sintered samples was determined by the linear intercept method.

For the in vitro bioactivity property examinations, the samples having the highest mechanical properties were ground with SiC papers of up to 1200 mesh and ultrasonically rinsed in acetone, absolute alcohol and deionised water five times in turn to remove any contamination and particulates. The solution was prepared by dissolving reagent grade sodium chloride (NaCl), potassium chloride (KCl), calcium chloride dihydrate ($\text{CaCl}_2\cdot 2\text{H}_2\text{O}$), magnesium chloride hexahydrate ($\text{MgCl}_2\cdot 6\text{H}_2\text{O}$), sodium hydrogen carbonate (NaHCO_3), dipotassium hydrogen phosphate trihydrate ($\text{K}_2\text{HPO}_4\cdot 3\text{H}_2\text{O}$), sodium sulfate (Na_2SO_4) in deionised water. Then the solution was buffered to a physiological pH of $7.32 \pm 1^\circ\text{C}$ by both hydrochloric acid (HCl) and tris (hydroxymethyl) aminomethane ($(\text{CH}_2\text{OH})_3\text{CNH}_2$). The in vitro bioactivity was evaluated by soaking the pellets, mounted vertically, in 40 mL of simulated body fluid (SBF) prepared according to Ref [39] for 14 and 28 days. After immersion in the SBF for various periods, the immersed samples were retrieved, gently rinsed with distilled water, and dried at 60°C for 1/2 day. The SEM analysis finally examined the surface of the samples, and the Ca/P ratio was calculated by energy dispersive X-ray diffraction (EDS) analysis.

RESULTS AND DISCUSSION

Figure 1 shows the X-ray diffraction (XRD) patterns of the pure HA depending on the sintering temperatures. 2.2 % of HA was decomposed into beta-tricalcium phosphate (β -TCP) after sintering at 1100°C , as shown in Table 2. The increase in the sintering temperature resulted in the decomposition of 3.8 % and 4.1 % of HA to β -TCP, respectively. Moreover, 1.6 % of HA

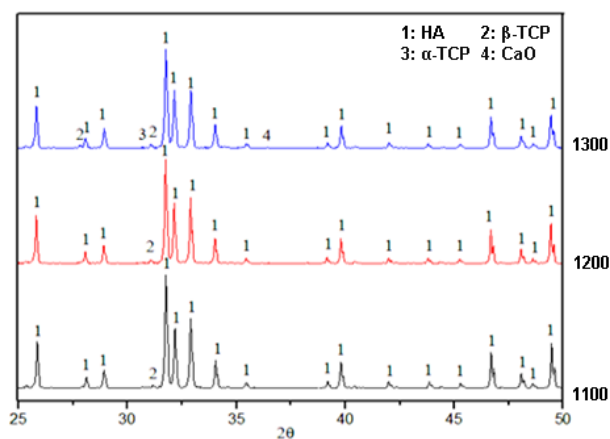


Figure 1. XRD patterns of the pure HA depending on the sintering temperatures.

Table 2. Chemical composition of the pure HA depending on the sintering temperature.

Sintering Temperature (°C)	Sample	Chemical composition (%)			
		HA	β -TCP	α -TCP	CaO
1100	Pure HA		2.2	-	-
1200			3.8	-	-
1300			4.1	1.6	0.1

decomposed into alpha-tricalcium phosphate (α -TCP) and 0.1 % into calcium oxide (CaO) when sintering was carried out 1300 °C. In other words, the decomposition rate of HA increased from 2.2 % to 4.8 % with the increase in the temperature. Its decomposition after sintering at 1300 °C was described by Chaki et al. [40] as seen in Reaction 1. ($\text{Ca}_3(\text{PO}_4)_2$ is β -TCP, and $\text{Ca}_3\text{P}_2\text{O}_8$ is α -TCP):

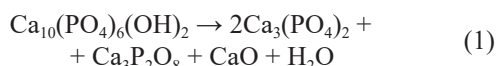


Figure 2 shows the XRD patterns of the HA-1M composites depending on the sintering temperatures. In the HA-1M composite, whitlockite and farringtonite phases were detected in addition to the main phase HA. The farringtonite ($\text{Mg}_3(\text{PO}_4)_2$) phase detected at a rate of 0.3 % at 1100 °C disappeared with the increasing temperature. It forms in the CaO-P₂O₅-MgO ternary system between 700 and 1100 °C [41] as the reaction between $(\text{PO}_4)^{3-}$ in $\text{Ca}_3(\text{PO}_4)_2$ and Mg^{2+} in MgO [42]. Incorporation of MgO leads to a gradual transformation of the HA in the whitlockite. However, if the MgO ratio exceeds 1 wt. %, it causes the formation of β -TCP together with whitlockite as the replacement of Ca by Mg in the HAP is limited. This is related to the size differences between the Mg^{2+} and Ca^{2+} (~0.28 Å) radii. Increasing the concentration of Mg in HA has the following effects on its properties: a) gradual decrease in the crystallinity; and b) increase in the extent of dissolution [43]. The content of whitlockite increased from 2.8 % to 6.5 %

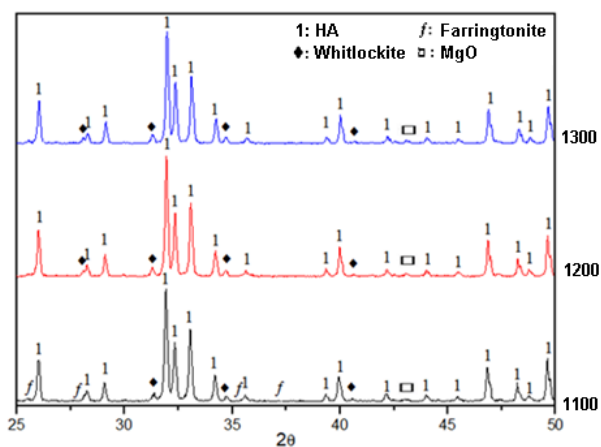


Figure 2. XRD patterns of the HA-1M composite depending on the sintering temperatures.

Table 3. Chemical composition of the HA-1M composite depending on the sintering temperature.

Sintering Temperature (°C)	Sample	Chemical composition (%)			
		HA	Whitlockite	MgO	Farringtonite
1100	HA-1M	96.7	2.8	0.2	0.3
1200		96.4	3.2	0.4	-
1300		93.0	6.5	0.5	-

with the increasing temperature (Table 3). The highest content of whitlockite in the present study is around 50 % lower than that of Ref [44]. Moreover, it was reported in the same study that increasing the MgO ratio from 1 wt. % to 20 wt. % resulted in the decomposition of 30 % of HA into β -TCP. The increase in the β -TCP content reduces the mechanical strength of HA ceramics and makes it unsuitable for surgical implant applications that require improved mechanical strength [45]. Whitlockite also contributes to the increase in the β -TCP \rightarrow α -TCP transformation temperature to around 1380 °C in HA-1 wt. % MgO composites [46]. HA and whitlockite have different atomic arrangements based on their hexagonal ($\text{P6}_3/\text{m}$) and rhombohedral (R3c) crystal structures, and exhibit different material properties. For example, while HA has greater stability in neutral pH conditions, whitlockite has higher stability in acidic conditions ($\text{pH} < 4.2$). As a result, whitlockite has higher solubility than HA in physiological conditions, and can continuously supply ions such as Mg^{2+} or PO_4^{3-} ions that can stimulate the ion channels at the membrane of stem cells, and enhance the osteogenic activity of cells. In addition, while HAP has a net neutral surface charge, whitlockite has a negatively charged surface which enables positively charged osteogenic proteins such as bone morphogenetic protein (BMP) to be adsorbed on its surface by electrostatic interaction [47].

Figure 3 and Tables 4-6 show the XRD patterns and the chemical compositions of the HA-1M-S composites, respectively. It is obviously seen that the

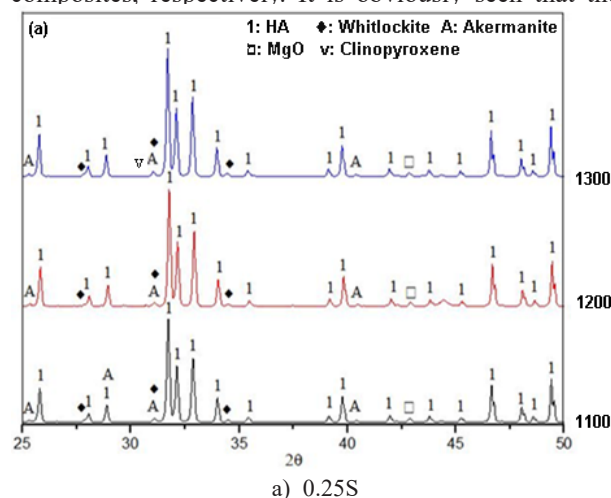


Figure 3. XRD patterns of HA-1M- composites.

continues on next page...

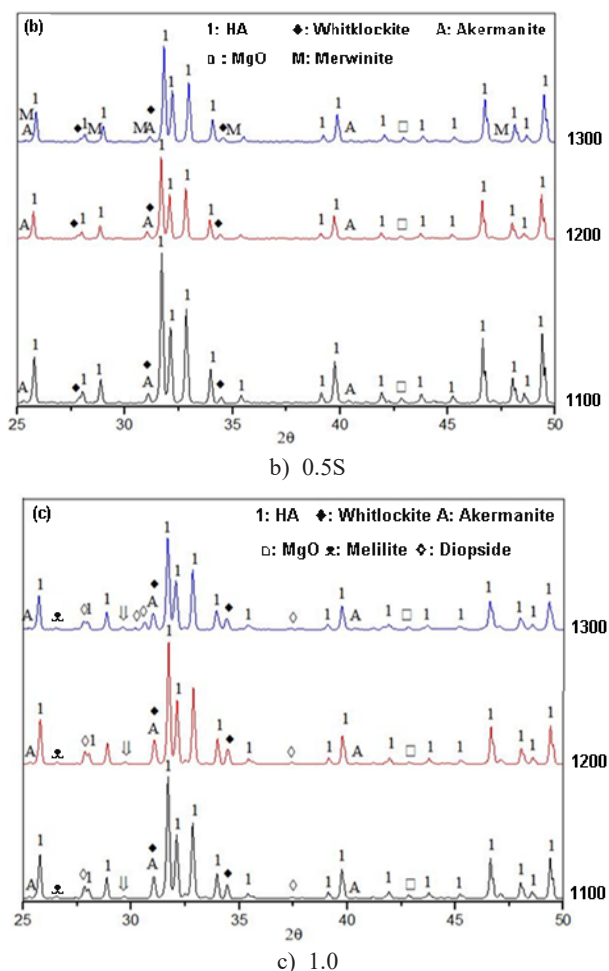


Figure 3. XRD patterns of HA-1M- composites.

type and percentages of the phases formed in HA-1M-S composites, as well as their chemical compositions, are affected by the SiO₂ ratio. In these composites, the farringtonite phase formed in the HA-1M composite was not detected. It is attributed to the formation of phases containing Ca-Mg-Si-O elements, such as akermanite, clinopyroxene, merwinite, melilite and diopside, formed in the SiO₂ added samples. In the case of the SiO₂ ratio of 0.25 wt. %, the whitlockite ratio increased from 3.5 % to 5.9 % with the increasing temperature, and it increased from 4.9 % to 7.8 % at an SiO₂ ratio of 0.5 wt. %. Increasing the SiO₂ ratio to 1 wt. % caused the whitlockite ratio to decrease and vary between 2.8 % and 4.6 %. It is clearly seen that the increase in the SiO₂ ratio to 1 wt. % triggers the formation of phases containing Ca-Mg-Si-O elements instead of the whitlockite phase in the microstructure. Akermanite is a member of CaO-MgOSiO₂-based bioceramics, belonging to a tetragonal crystal system, space group P-4₂m and Z = 2. Additionally, it possesses superior mechanical properties to those of HA and β-TCP [48]. It is formed by the eutectic transformation at 1376 °C in the CaO-MgO-SiO₂ ternary system [49] and maintains its stability up to room temperature [50]. Clinopyroxene crystallises in the (100) direction as subhedral grains as a result of the dissolution of diopside-enstatite in the CaO-MgO-SiO₂ system [51, 52]. Its presence was also confirmed by Ref [53], where Mg and Si were co-substituted into HA. Merwinite is a bioceramic in the CaO-MgO-SiO₂ system [54], which occurs at 1410 ± 5 °C after the eutectic

Table 4. Chemical composition of the HA-1M-0.25S composite depending on the sintering temperature.

Sintering Temperature (°C)	Sample	Chemical composition (%)				
		HA	Whitlockite	Akermanite	MgO	Clinopyroxene
1100	HA-	95.7	3.5	0.3	0.5	-
1200	-1M-	93.2	4.1	1.9	0.8	-
1300	-0.25S	90.6	5.9	2.4	0.9	0.2

Table 5. Chemical composition of the HA-1M-0.5S composite depending on the sintering temperature.

Sintering Temperature (°C)	Sample	Chemical composition (%)				
		HA	Whitlockite	Akermanite	MgO	Merwinite
1100	HA-1M-0.5S	94.3	4.9	0.5	0.3	-
1200		93.0	5.1	1.2	0.7	-
1300		86.6	7.8	1.8	0.8	3.0

Table 6. Chemical composition of the HA-1M-1S composite depending on the sintering temperature.

Sintering Temperature (°C)	Sample	Chemical composition (%)					
		HA	Whitlockite	Akermanite	MgO	Melilite	Diopside
1100	HA-1M-0.5S	93.6	2.8	3.1	0.2	0.1	0.2
1200		90.7	3.4	4.6	0.4	0.4	0.5
1300		83.3	4.6	10.0	0.5	0.7	0.9

transformation (liquid akermanite + merwinite) [55]. The CaO/MgO molar ratio is in the range of 4.02 - 4.24, and the MgO/SiO₂ molar ratio is in the range of 0.33 - 0.38 in the merwinite [56]. Melilite crystallises in a tetragonal crystal structure, a layered structure in which Mg and Si are in a corner sharing tetrahedral coordination [57]. It is formed by the dissolution of MgO in Ca₂SiO₄ at about 1320 °C in the CaO-MgO-SiO₂ system when Mg is at an atomic rate of 3.89 % [58], and it nucleates in the interface region of akermanite and diopside during the transformation of the liquid into akermanite and diopside phases [59]. Diopside is a member of the clinopyroxene mineral family that possess a single chain silicate structure and crystallises to form a solid solution with other cations available for substitution for calcium and magnesium. It has been proposed for use in bone surgery due to its high bending and compression strength which is stronger than human cortical bones [60]. According to the literature, all the crystalline phases indicate they have the bioactivity property, since they induce the formation of hydroxyapatite on the ceramic body in the SBF solution [61].

Figure 4 shows the shrinkage of the pure HA, HA-1M and HA-1M-S composites depending on the sintering temperature. The increase in the sintering temperature contributed to the increase in the shrinkage rates of the pure HA (13.53 ± 0.50 to 18.20 ± 0.62 %) and HA-1M composite (12.82 ± 0.25 to 18.45 ± 0.61 %). The shrinkage in the HA-1M-0.25S (from 17.17 ± 1.15 % to 18.51 ± 1.31 %) and HA-1M-0.5S (from 17.00 ± 0.77 % to 19.58 ± 1.21 %) composites reached the highest values with the increasing temperature, however; the highest shrinkage for the HA-1M-1S composite was determined to be 17.436 ± 0.668 % at 1200 °C. The sintering of the SHA-1M-1S composite at 1300 °C caused a reduction in the shrinkage from the highest value to 17.16 ± 0.76 %. This is related to the formation of diopside in this composite after sintering at 1300 °C, as can be seen in Figure 3c. Because its coefficient of thermal expansion (3.33 × 10⁻⁶ K⁻¹ [62]) is much lower than the other phases, i.e., HA (13.6 × 10⁻⁶ K⁻¹ [63]), whitlockite

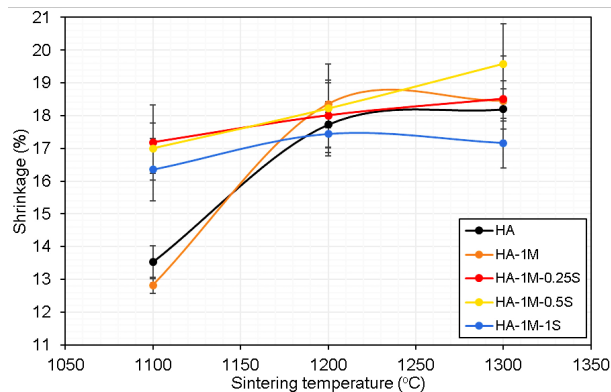


Figure 4. Shrinkage of the pure HA, HA-1M and HA-1M-S composites depending on the sintering temperature.

(11.1 × 10⁻⁶ K⁻¹ [64], akermanite (8.8 × 10⁻⁶ K⁻¹ [65], melilite (5.4 × 10⁻⁶ K⁻¹ [66]), and MgO (8.0 × 10⁻⁶ K⁻¹ [67]). In addition, the shrinkage of the HA-1M-1S composites was determined to be lower than the other SiO₂ added composites for all the sintering temperatures. This is due to the fact that the clinopyroxene (1205 °C [68]) and merwinite (1420 °C [69]) phases formed in the HA-1M-0.25S and HA-1M-0.5S composites have a lower melting point compared to the melilite (1576 °C [70]) and diopside (1715 °C [71]) phases, that is, they contribute to the increase in the sinterability behaviour of the HA-1M composite.

Figure 5 shows the density, porosity and relative density of HA and the composites depending on the sintering temperature. The density of HA without any

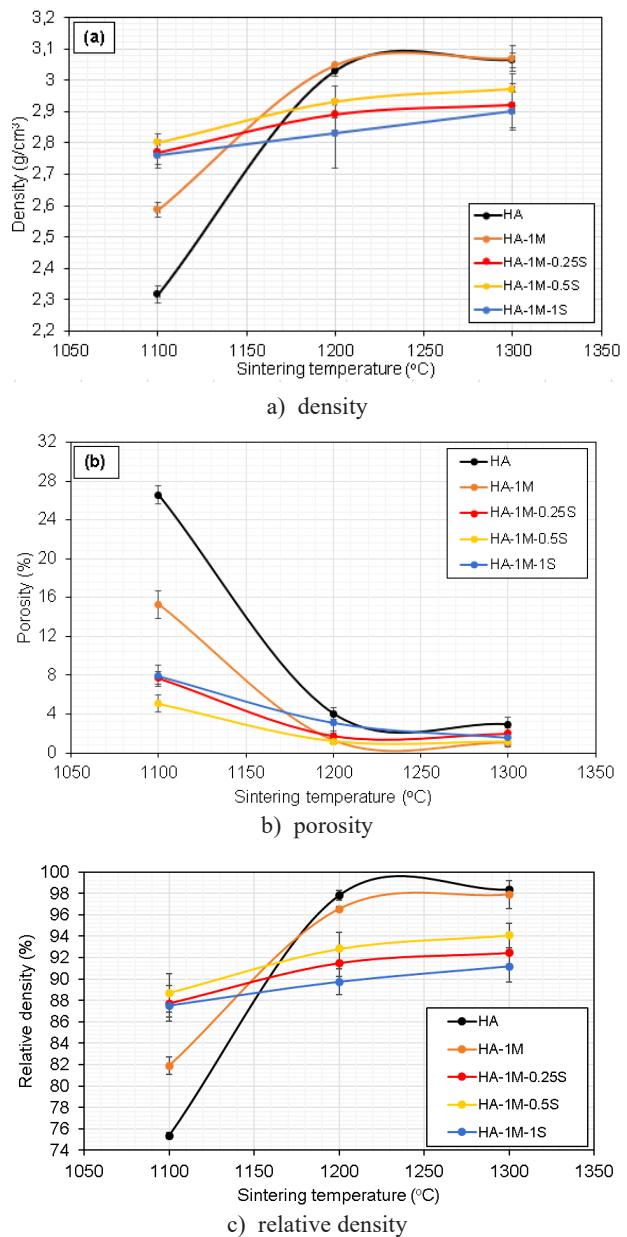


Figure 5. The density (a), porosity (b) and relative density (c) of HA and the composites depending on the sintering temperature

additives measured as $2.316 \pm 0.028 \text{ g}\cdot\text{cm}^{-3}$ at $1100 \text{ }^\circ\text{C}$ increased to $3.029 \pm 0.018 \text{ g}\cdot\text{cm}^{-3}$ at $1200 \text{ }^\circ\text{C}$ and $3.064 \pm 0.024 \text{ g}\cdot\text{cm}^{-3}$ at $1300 \text{ }^\circ\text{C}$. Similar behaviour, i.e., an increase in density with an increasing temperature, was observed for HA-1M and its density increased from 2.586 ± 0.025 to $3.068 \pm 0.041 \text{ g}\cdot\text{cm}^{-3}$. The densities of the SiO_2 added samples were determined to vary between 2.760 ± 0.040 and $2.970 \pm 0.050 \text{ g}\cdot\text{cm}^{-3}$. The density of these composites at $1100 \text{ }^\circ\text{C}$ is higher than that of HA and the HA-1M composite, whereas they are lower at 1200 and $1300 \text{ }^\circ\text{C}$. The attainment of a lower density in the SiO_2 added samples when sintering is performed at 1200 and $1300 \text{ }^\circ\text{C}$ is due to the formation of Ca-Mg-Si-O containing phases, most of which have a lower theoretical density than HA, MgO and whitlockite (Table 7).

Table 7. The theoretical density of the phases that occurred in the HA-1M-S composites.

Phase	Theoretical density ($\text{g}\cdot\text{cm}^{-3}$)	Reference
Akermanite	2.94	[72]
Clinopyroxene	2.91	[73]
Melilite	2.92	[74]
Merwinite	3.34	[75]
Diopside	3.26	[76]
Whitlockite	3.12	[77]

The attainment of a higher density in the SiO_2 added samples when sintering is performed at $1100 \text{ }^\circ\text{C}$ is due to the lower melting points of SiO_2 ($1726 \text{ }^\circ\text{C}$ [78]) compared to MgO ($2852 \text{ }^\circ\text{C}$ [79]). This led to an increase in the sinterability between HA and MgO particles at the sintering temperature of $1100 \text{ }^\circ\text{C}$. Therefore, the porosity ratios of the SiO_2 added samples at this temperature are considerably lower than the pure HA and HA-1M composite (Figure 5b). It was calculated as $26.589 \pm 0.895 \%$ for the pure HA and $15.297 \pm 1.430 \%$ for HA-1M composite, but decreased to the lowest value with $5.079 \pm 0.907 \%$ in the $0.5 \text{ wt. } \%$ SiO_2 added sample. Also, the porosity ratios of HA-1M-0.5S at 1200 and $1300 \text{ }^\circ\text{C}$ measured as $1.166 \pm 0.180 \%$ and $1.129 \pm 0.456 \%$, respectively, and they were found to be lower than the other HA-1M-S composites. The porosity of the pure HA at these temperatures was measured as $4.018 \pm 0.595 \%$ and $2.912 \pm 0.769 \%$, respectively. The porosity ratios in the HA-1M composites after sintering above $1100 \text{ }^\circ\text{C}$ were measured as $1.257 \pm 0.282 \%$ and $1.019 \pm 0.185 \%$, respectively. Sintering of HA-1M at $1200 \text{ }^\circ\text{C}$ with the addition of SiO_2 at an amount of 0.25 and $1.0 \text{ wt. } \%$ led to its porosity increasing from $1.257 \pm 0.282 \%$ to $1.743 \pm 0.465 \%$ and to $3.118 \pm 0.821 \%$. On the other hand, the sintering of the HA-1M composite at $1300 \text{ }^\circ\text{C}$ increased its density from $1.019 \pm 0.185 \%$ to a maximum of $1.975 \pm 0.789 \%$. It is clearly seen that the addition of SiO_2 caused a slight increase in the porosity ratio of the HA-1M composite. Similar

behaviour has also confirmed for co-(0.65 - $1.38 \text{ wt. } \%$) Mg/(0.92 - $1.73 \text{ wt. } \%$)Si substituted HA [80]. It has been proven that a slight increase in the porosity ratio of the HA-1M composite with the addition of SiO_2 contributes to a significant increase in the osteogenesis, osseointegration, and bone mineralisation of titanium implants after 6, 10 and 14 weeks of implantation in rat distal femoral defects [81]. Bioceramics with three different components may have a lower sintered density and, therefore, possibly slightly higher porosity than bioceramics with two different components, however; this tends to favour the biomineralisation process by accelerating the release of Ca^{2+} and PO_4^{3-} and their supersaturation levels in the environment. [82]. Bioceramics containing biocompatible phases with a relative density at about 90% are preferred in biomedical applications because they can provide sufficient mechanical properties and contribute to the interaction in the implant-bone interface region [83]. The relative density of the pure HA increased from 75.365 ± 0.789 to $98.353 \pm 0.176 \%$ with the increasing temperature. In HA-1M, it increased from 81.885 ± 0.882 to $97.885 \pm 1.312 \%$. The relative density varies between 87.519 ± 1.044 and $88.701 \pm 1.783 \%$, which was obtained by sintering at $1100 \text{ }^\circ\text{C}$ and adding SiO_2 . It was between 89.739 ± 1.239 and $94.086 \pm 1.138 \%$ above $1100 \text{ }^\circ\text{C}$ in the HA-1M-S composites. However, the relative density of the HA-1M-S composites above $1100 \text{ }^\circ\text{C}$ are higher than commercial inert glass added HA- Al_2O_3 and HA- ZrO_2 composites [84]. The addition of Al_2O_3 [85], ZrO_2 [86], and commercial inert glass [87] causes an increase in the β - and/or α -TCP content of HA and a decrease in its sinterability. Additional problems related to the sintering of HA/glass composites are the formation of micropores due to the release of OH^- groups from HA during thermal treatment, the local shrinkage of glass through liquid-phase sintering, and the specific volume change caused by the β -TCP \rightarrow α -TCP transformation [88].

Figure 6 shows the hardness, fracture toughness and brittleness index of HA and the composites depending on the sintering temperature. The increase in the sintering temperature contributed to the increase in the hardness of the pure HA and allowed it to increase from 154.10 ± 5.40 to $499.20 \pm 12.39 \text{ HV}$. The highest hardness of HA is in agreement with Ref [89]. It is believed that the higher density played a role in producing higher hardness values where an increase in the density leads to an increase in the hardness [90]. The highest fracture toughness for the pure HA was measured as $0.96 \pm 0.05 \text{ MPa}\cdot\text{m}^{1/2}$ at $1100 \text{ }^\circ\text{C}$ and decreased to $0.71 \pm 0.06 \text{ MPa}\cdot\text{m}^{1/2}$ with the increasing temperature. Similar behaviour was also confirmed by Ref [91]. A decrease in the fracture toughness with an increasing grain size is usually observed in pure HA ceramics when the mechanism is transgranular because the major contribution to cracking resistance is related to the crossing of the grain boundaries [92]. Increasing

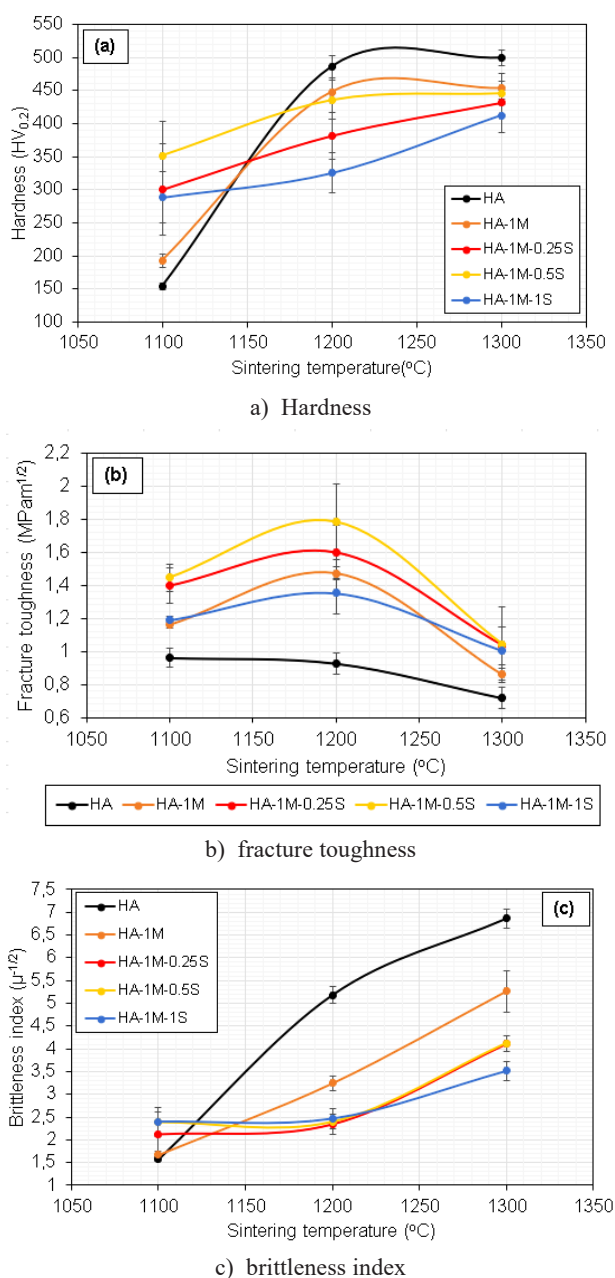


Figure 6. Hardness (a), fracture toughness (b) and brittleness index (c) of HA and the composites depending on the sintering temperature.

in the sintering temperature caused a significant increase in the brittleness index of the pure HA (from 1.57 ± 0.05 to $6.86 \pm 0.21 \mu^{-1/2}$). The hardness (from 192.9 ± 10.65 to 453.0 ± 022.82 HV) and brittleness index (from 1.67 ± 0.09 to $5.26 \pm 0.46 \mu^{-1/2}$) of the HA-1M composite also increased with the increasing temperature, but the highest fracture toughness was measured as $1.47 \pm 0.04 \text{ MPa}\cdot\text{m}^{1/2}$ when sintering was carried out at 1200°C . In the HA-1M-S composites, the highest hardness and fracture toughness were calculated as 445.90 ± 17.10 HV and $1.78 \pm 0.22 \text{ MPa}\cdot\text{m}^{1/2}$, respectively. They are obtained as a result of sintering at 1300 and 1200°C

and belong to the HA-1M-0.5S composite. Sintering at 1300°C caused its fracture toughness to drop to $1.04 \pm 0.22 \text{ MPa}\cdot\text{m}^{1/2}$. Its brittleness index increased from 2.39 ± 0.35 to $4.12 \pm 0.45 \mu^{-1/2}$ with an increase in the sintering temperature. The hardness increased from 300.40 ± 68.60 to 431.70 ± 18.24 HV for HA-1M-0.25S, and from 288.68 ± 38.40 to 411.96 ± 24.81 HV for HA-1M-1.0S. The highest fracture toughness of the HA-1M-0.25S and HA-1M-1.0S composites was obtained at 1200°C and calculated as 1.60 ± 0.16 and $1.35 \pm 0.12 \text{ MPa}\cdot\text{m}^{1/2}$, respectively. As a result of sintering at 1300°C , the fracture toughness of these composites decreased to 1.03 ± 0.16 and $1.00 \pm 0.14 \text{ MPa}\cdot\text{m}^{1/2}$, respectively. The brittleness index of these composites increased with the increasing temperature, which was measured as 2.11 ± 0.48 , 2.34 ± 0.21 and $4.11 \pm 0.45 \mu^{-1/2}$ for the HA-1M-0.25S composite and as 2.39 ± 0.31 , 2.46 ± 0.22 and $3.51 \pm 0.20 \mu^{-1/2}$ for the HA-1M-1.0S composite. With the addition of SiO_2 at an amount of 0.5 wt. %, a 20 % increase in the highest fracture toughness and a 35 % decrease in the brittleness index of HA-1M could be achieved when sintering was carried out at 1200 and 1300°C . It is thought that the improvement in the fracture toughness of HA-1M composites by the addition of SiO_2 may be related to three different mechanisms: The more grain boundaries consume more energy of the crack during its sintering granular propagation as the grain size decreased [93]. The chemical bonding of SiO_2 is a covalent binding, whereas that of MgO is an ion binding. The covalent binding is comparatively strong, whereas the ion binding is comparatively weak [94]. The addition of SiO_2 to the HA-1M composite increased the bond between the MgO and HA particles by providing the formation of intergranular phases, such as akermanite ($1.83 \text{ MPa}\cdot\text{m}^{1/2}$ [95]), merwinite ($2.68 \text{ MPa}\cdot\text{m}^{1/2}$ [96]), clinopyroxene ($2.0 \text{ MPa}\cdot\text{m}^{1/2}$ [97] and diopside ($3.5 \text{ MPa}\cdot\text{m}^{1/2}$ [64], which have higher fracture toughness than whitlockite, farringtonite and HA, and caused the propagation of cracks formed during micro-indentation along the grain boundaries. It was concluded that there may be several reasons for the 35 % decrease in the brittleness index of HA-1M with the addition of SiO_2 after sintering at 1200 and 1300°C . As the hardness increases, the brittleness index of the material increases [38]. For this reason, the HA and HA-1M composites with higher microhardness values are the most prone to fracture. The other reason is that the intergranular phases formed by the addition of SiO_2 encourage grain formation with homogeneous distribution as shown in Figure 8. In a previous study, the same behaviour was also confirmed in the HA doped with 5 % moles of Mg, Mn or Zn [98]. It has been reported that a material intended to be used as a bone implant material should have a brittleness index lower than $4.3 \mu^{-1/2}$ [99]. It is seen that SiO_2 added samples meet this requirement.

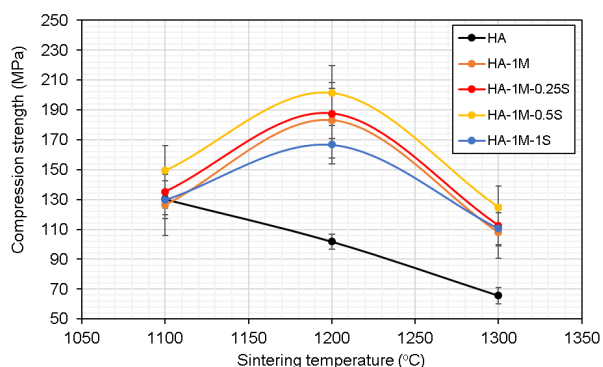


Figure 7. Compression strength of the HA and the composites.

Figure 7 shows the compression strength of HA and the composites. The increase in the sintering temperature caused the compressive strength of the pure HA to decline from 130.2 ± 6.22 to 65.6 ± 5.59 MPa. Traditional sintering of HA requires a temperature of over 1100°C for densification. However, the high temperature not only consumes time and energy, but also causes HA to lose hydroxyl groups and destroy its structural stability [100]. The average grain size of pure HA dramatically increased from 0.473 to $17.167\ \mu\text{m}$ with the increasing sintering temperature, as shown in Figure 7. With an increase in grain size, the compression strength of the sintered HA compacts decreases [101]. It is also attributed to the presence of microcracking due to mismatch in the thermal expansion behaviour of the secondary phases, i.e., TCPs and CaO, in the HA compacts [102]. Microcracking in HA ceramics is also observed when the grain size of HA exceeds a certain critical value. It was calculated as $0.4\ \mu\text{m}$ by Ref [103]. The formation of microcracks in HA ceramics also causes a reduction in the cross-sectional area and, thus, causes a decrease in the resistance to compression load [104]. Briefly, the compression strength of the pure HA decreased with the increasing temperature due to three factors, namely microcracking due to the thermal expansion mismatch and exceeding the critical grain size and reduction in the cross-sectional area. Due to the minimisation of these factors, the highest compressive strengths of the HA-1M

and HA-1M-S composites are higher than that of the pure HA. The compressive strength of the HA-1M composite of 126.5 ± 20.5 MPa at 1100°C increased to its highest value of 183 ± 25.09 MPa at 1200°C , but decreased to 108 ± 17.51 MPa at 1300°C . Similar behaviour, that is, obtaining the highest compressive strength at 1200°C and decreased compressive strength at 1300°C , was also observed in the HA-1M-S composites. The microstructure of samples sintered at 1300°C show abnormal grain growth compared to the samples sintered at 1200°C , which may be the reason for the reduction in the strength [105]. The compressive strength of the HA-1M-0.25S composite at 1100 , 1200 and 1300°C was calculated as 135.2 ± 15.42 , 187.59 ± 16.80 and 112.43 ± 13.76 MPa, respectively. While the compressive strength of the HA-1M-0.5S composite is 149.27 ± 16.95 , 201.53 ± 18.01 and 124.61 ± 14.28 MPa, and they are 129.83 ± 12.59 , 166.72 ± 12.84 and 110.55 ± 10.76 MPa for the HA-1M-1S composite, respectively. There are two reasons why the 0.5 wt. % SiO_2 added sample has a higher compressive strength than that of HA-1M: First, the akermanite (210 MPa [106]) formed in these composites has a higher compressive strength than that of whitlockite (306.25 kPa [107]). Second, its average grain size is about 25 % less than that of HA-1M, as shown in Figure 8. With a decrease in the grain size, the fracture toughness and compressive strength of HA based ceramics increase [108]. The highest compressive strength of the HA-1M-S composites is also compatible with 100-230 MPa, but its fracture toughness is less than $2\text{-}12\ \text{MPa}\cdot\text{m}^{1/2}$, which are desired limits for implants requiring load resistance in the human body [109].

The SEM images of HA-1M and HA-1M-S composites are shown in Figure 9. They are composed of closely packed particles and well-defined grain boundaries without microcracking. The SiO_2 additives also contribute the grain growth inhibition in the HA-1M composite. However, the addition of SiO_2 at an amount of 1 wt. % caused a decrease in the sinterability of the HA-1M composite. It is also composed of porosities and grains with heterogeneous size distribution.

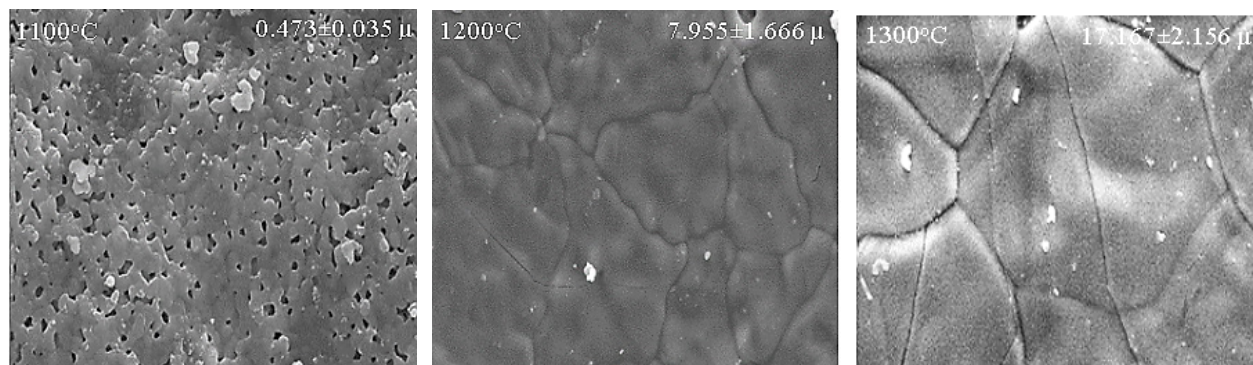


Figure 8. SEM images of the pure HA sintered at 1100 , 1200 and 1300°C , respectively.

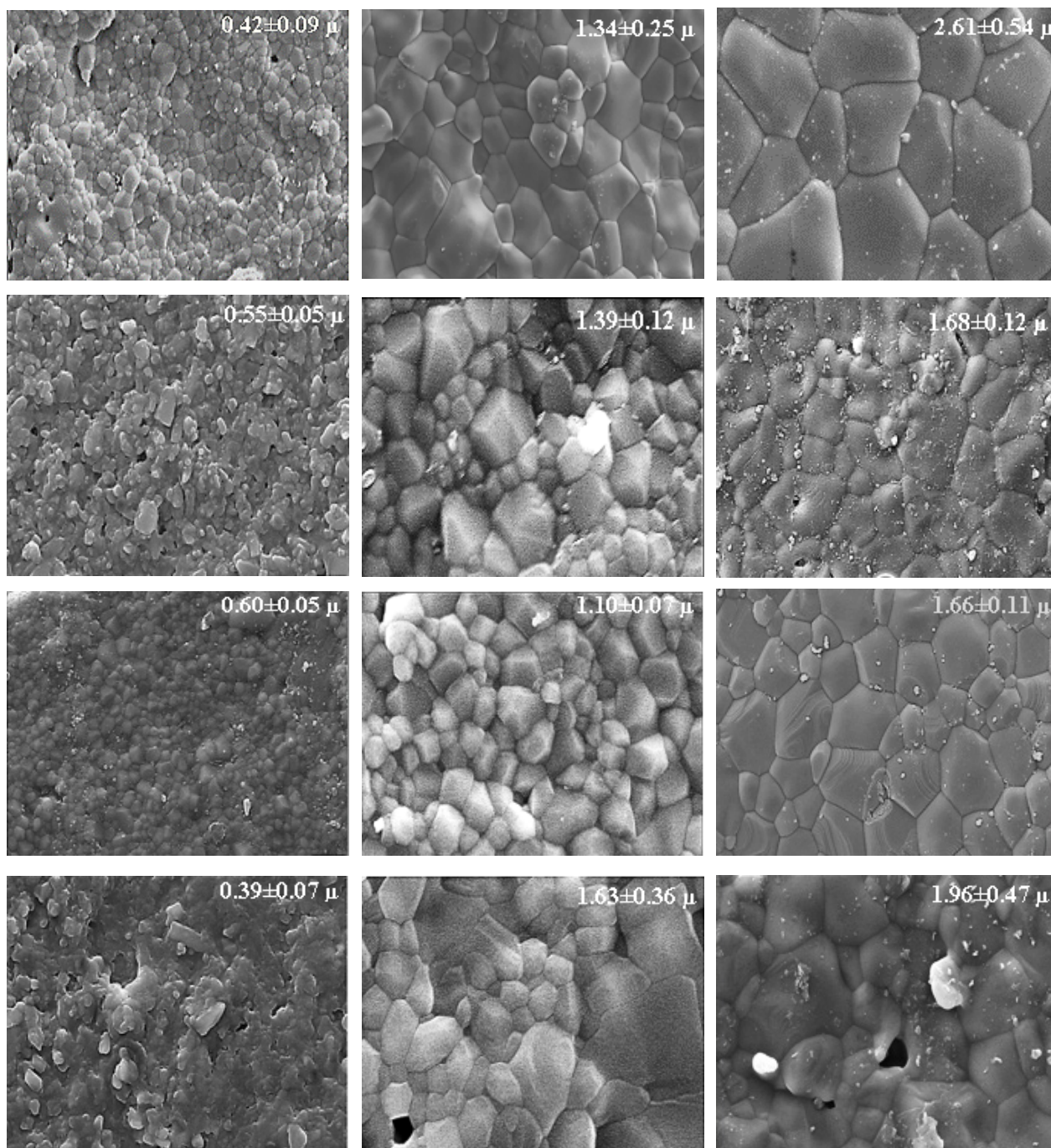


Figure 9. SEM images of the HA-1M and HA-1M-S composites.

As seen in Figure 10; after 7 days of the SBF test, an apatite layer started to form on the pure HA surface having a cube-shaped form, and its surface was completely covered with the apatite layer after 28 days of the SBF test. As a result of the EDS examinations, the Ca/P molar ratio was calculated as 1.70, 1.61, 1.39 and 1.24. As reported by Ref [110], the Ca/P molar ratio of the apatite layer formed on the surface of a biomaterial, which has the mechanical properties that can be used in bone regeneration applications, after the SBF test, it

should be between 1.2 and 2.0. In addition, the presence of elements such as sodium and magnesium on the pure HA surface was detected. It is due to the precipitation of ions such as magnesium, sodium and chlorine from the SBF solution during the formation of the apatite layer on the surface of HA ceramics immersed in the SBF solution [111]. As can be seen in Figure 11; the ratio of the apatite layer formed on the surface of the HA-1MgO composite showed a significant decrease compared to HA for all the SBF times, and, as a result of the EDS analysis, the Ca/P

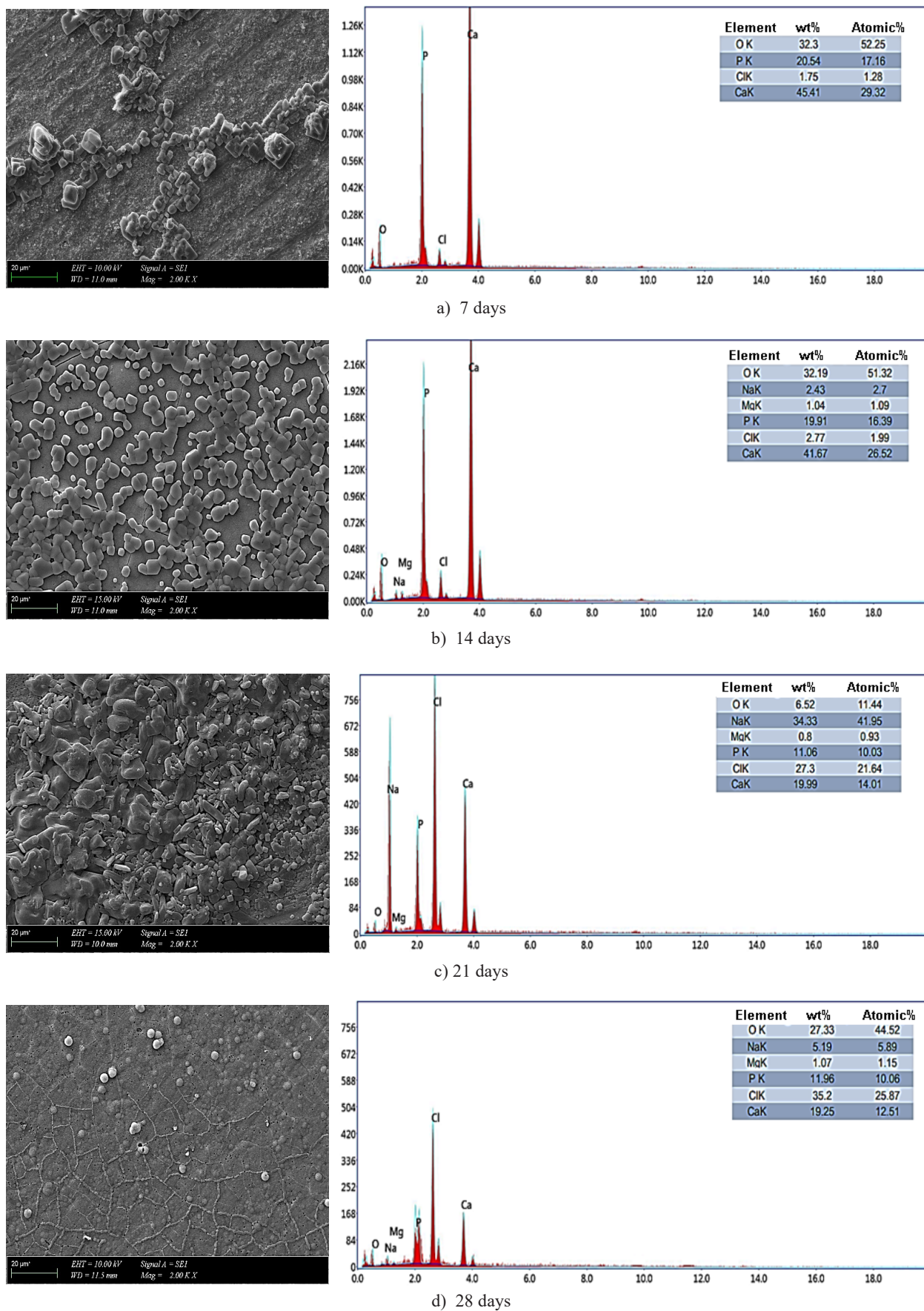


Figure 10. SEM and EDS analyses of HA for (a) 7, (b) 14, (c) 21 and (d) 28 days of immersion in the SBF solution.

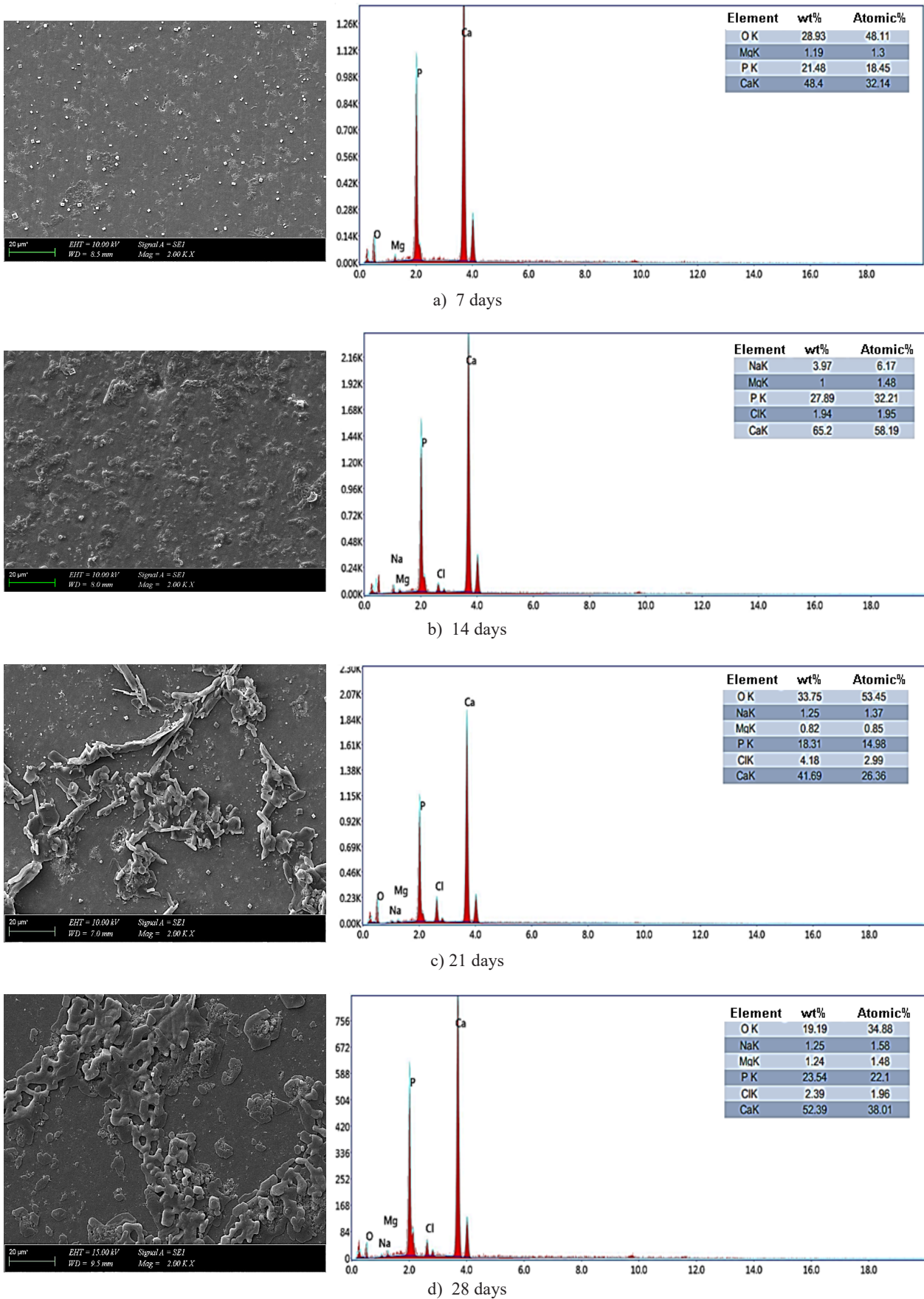


Figure 11. SEM and EDS analyses of HA-1M for (a) 7, (b) 14, (c) 21 and (d) 28 days of immersion in the SBF solution.

molar ratio of the apatite layer formed on the surface of the HA-1M composite was 1.74, 1.80, 1.75 and 1.71. It has been stated that the Ca/P molar ratio of the apatite layer formed on the surface of borophosphate bioglass for 0.5 wt. % MgO is 2.063 and 2.91 for 3 wt. % MgO [112]. As can be seen from the SEM microstructure images of HA-1M-0.5S subjected to the SBF test (Figure 12); at the end of the 7th day, the apatite layer crystallised in a cubic form. As a result of the 14- and 21-day SBF test, it has a denser and dendritic structure compared to the HA-1M composite. After the 28 days of the SBF test, its surface was completely covered with the apatite layer, that is, it

contributed to the increase of the bioactivity of the HA-1M composite. The Ca/P molar ratio of the apatite layer formed on the surface of this composite was 1.69, 1.76, 1.72 and 1.93. Studies on bioactive systems containing Si, Ca, and P ions show that biomaterials containing these elements have better in vitro bioactive behaviour compared to conventional bioactive glasses, and these Si-containing biomaterials may be better candidates for drug release and bone regeneration. It has been stated that the addition of Si to systems containing Ca, Mg, P ions increases the bioactivity of the system [113].

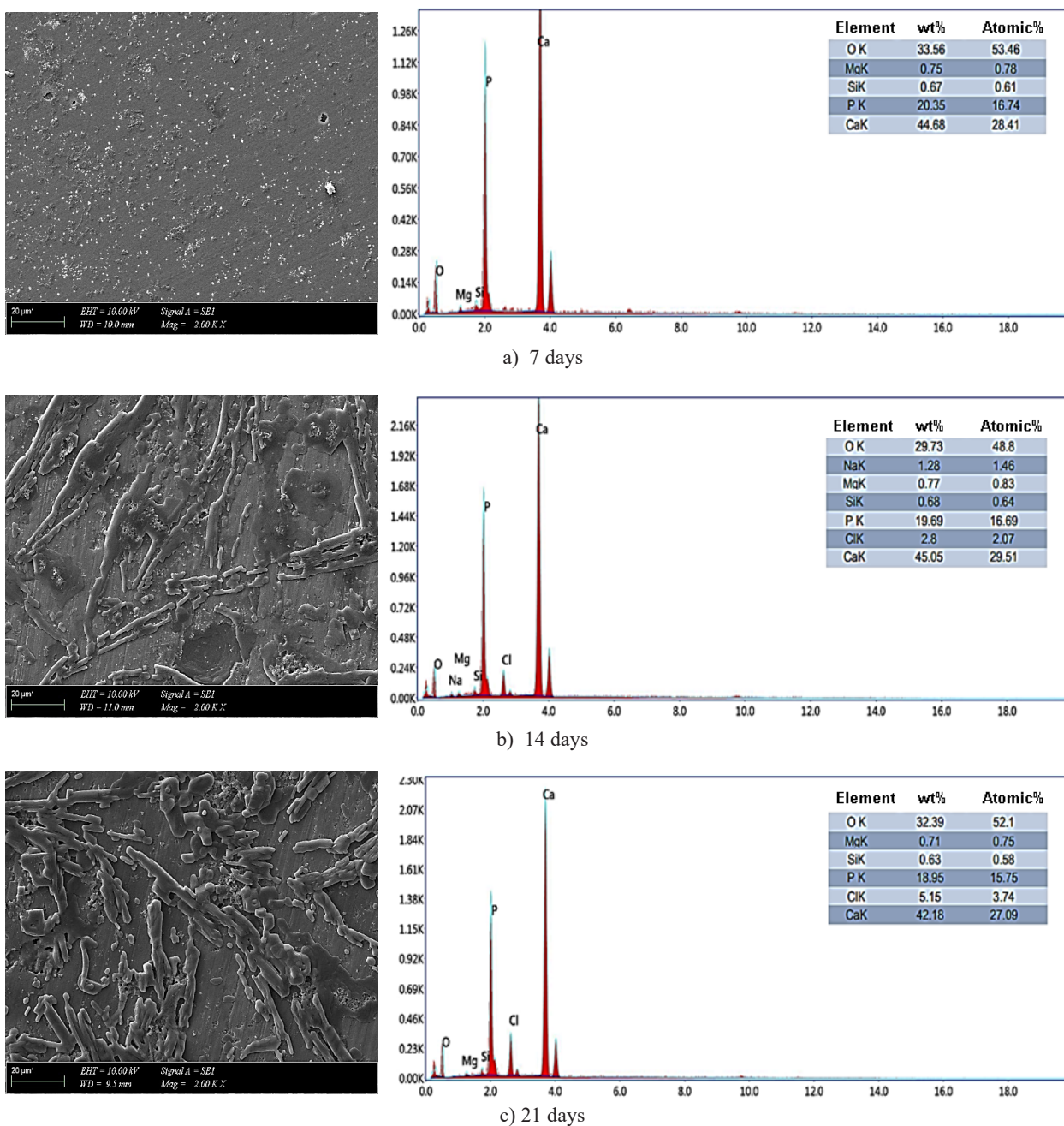


Figure 12. SEM and EDS analyses of HA-1M-0.5S composite for (a) 7, (b) 14, (c) 21 and (d) 28 days of immersion in the SBF solution. *continues on next page ...*

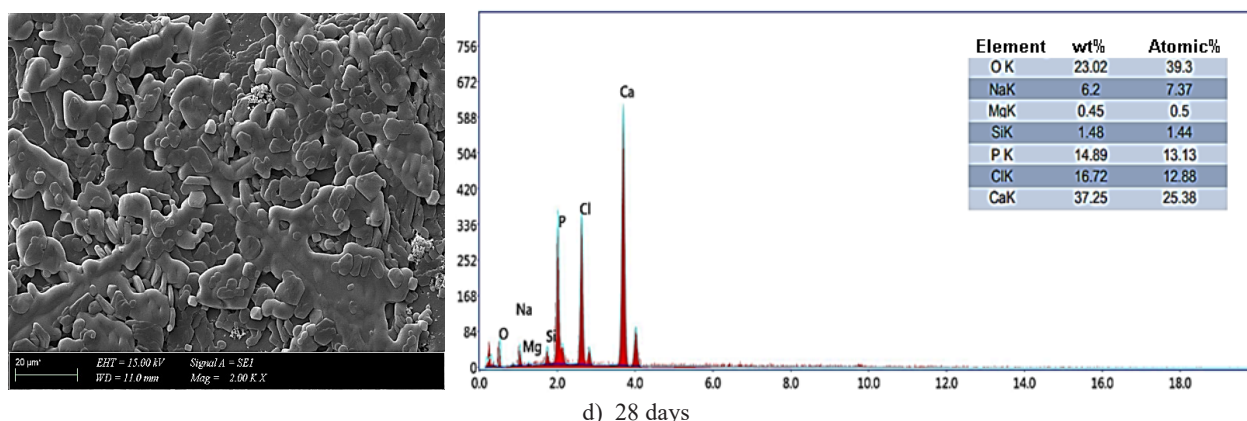


Figure 12. SEM and EDS analyses of HA-1M-0.5S composite for (a) 7, (b) 14, (c) 21 and (d) 28 days of immersion in the SBF solution.

The akermanite in the HA-1M-0.5S composite is a silicate-based phase, and its presence in a material used in clinical applications is preferred since it contributes to the bone regeneration. The Ca, Mg and Si released would be beneficial to accelerate bone tissue regeneration and remodelling. It has been reported that the Mg, Ca and Si ions release from bioceramics for bone regeneration, as akermanite, decreases the immune responses caused by macrophages both in vitro and in vivo [114]. It also plays an important role in the development of healthy bones and connective tissues and provides rapid dissolution of magnesium and calcium. Deprotonation of silica from akermanite triggers not only growth, but also precipitation of apatite crystals [115]. Therefore, it can be said that the bioactivity of HA-1M-0.5S is higher than HA-1M.

CONCLUSIONS

In the present study, the effect of an SiO₂ additive on the properties of an HA-1 wt. % MgO composite was investigated and the following results were obtained:

1. HA without additives is composed of β -TCP, α -TCP and CaO. In the HA-1M composite, whitlockite and farringtonite phases were detected.
2. HA without an additive showed shrinkage of 18.20 ± 0.62 % when sintering was carried out 1300 °C. It increased to 18.45 ± 0.61 % and 19.58 ± 1.21 % for the HA-1M and preferred HA-1M-0.5S composites, respectively.
3. Increasing the sintering temperature contributed to an increase in the density of HA from 2.316 ± 0.028 g·cm⁻³ to 3.029 ± 0.018 g·cm⁻³. The highest density for HA-1M was calculated as 3.068 ± 0.041 g·cm⁻³. The densities of the HA-1M-S composites were determined to vary between 2.760 ± 0.040 and 2.970 ± 0.050 g·cm⁻³.
4. The porosity of 26.589 ± 0.895 % of HA decreased to 2.912 ± 0.769 % after sintering at 1300 °C. It

was 15.297 ± 1.430 % for HA-1M at 1100 °C and decreased to 1.257 ± 0.282 % at 1200 °C and 1.019 ± 0.185 % at 1300 °C. The addition of SiO₂ caused a slight increase in the porosity of HA-1M at elevated temperatures.

5. The relative density of HA increased from 75.365 ± 0.789 to 98.353 ± 0.176 % with an increasing temperature. In HA-1M, it increased from 81.885 ± 0.882 to 97.885 ± 1.312 %. The relative density varied between 87.519 ± 1.044 and 88.701 ± 1.783 %, which was obtained by sintering at 1100 °C and adding SiO₂, where it was between 89.739 ± 1.239 and 94.086 ± 1.138 % above 1100 °C in the HA-1M-S composites.
6. The hardness of HA increased from 154.10 ± 5.40 to 499.20 ± 12.39 HV. The highest fracture toughness for HA was measured as 0.96 ± 0.05 MPa·m^{1/2} at 1100 °C, but decreased to 0.71 ± 0.06 MPa·m^{1/2} with the increasing temperature. The brittleness index of HA increased from 1.57 ± 0.05 to 6.86 ± 0.21 $\mu^{-1/2}$. The hardness and brittleness index of HA-1M also increased with the increasing temperature, but the highest fracture toughness was measured as 1.47 ± 0.04 MPa·m^{1/2} after sintering at 1200 °C. The hardness increased from 300.40 ± 68.60 to 431.70 ± 18.24 HV for the HA-1M-0.25S composite, and from 288.68 ± 38.40 to 411.96 ± 24.81 HV for the HA-1M-1.0S composite. The highest fracture toughness of HA-1M-0.25S as 1.60 ± 0.16 MPa·m^{1/2} and HA-1M-1.0S as 1.35 ± 0.12 MPa·m^{1/2} was obtained at 1200 °C, but at the sintering temperature of 1300 °C, they decreased to 1.03 ± 0.16 and 1.00 ± 0.14 MPa·m^{1/2}, respectively. The brittleness index of these composites increased with the increasing temperature, which was measured as 2.11 ± 0.48 , 2.34 ± 0.21 and 4.11 ± 0.45 $\mu^{-1/2}$ for the HA-1M-0.25S composite and as 2.39 ± 0.31 , 2.46 ± 0.22 and 3.51 ± 0.20 $\mu^{-1/2}$ for the HA-1M-1.0S composite. With the addition of SiO₂ at an amount of 0.5 wt. %, a 20 % increase in the highest fracture toughness

and a 35 % decrease in the brittleness index of HA-1M could be achieved when sintering was carried out at 1200 and 1300 °C, respectively.

7. The compression strength of HA decreased from 130.2 ± 6.22 to 65.6 ± 5.59 MPa with the increase in the sintering temperature. The compressive strength of the HA-1M composite of 126.5 ± 20.5 MPa at 1100 °C increased to its highest value of 183 ± 25.09 MPa at 1200 °C, but decreased to 108 ± 17.51 MPa at 1300 °C. Similar behaviour was also observed in the HA-1M-S composites. The compressive strength of the HA-1M-0.25S composite at 1100, 1200 and 1300 °C was calculated as 135.2 ± 15.42 , 187.59 ± 16.80 and 112.43 ± 13.76 MPa, respectively. While the compressive strength of the HA-1M-0.5S composite is 149.27 ± 16.95 , 201.53 ± 18.01 and 124.61 ± 14.28 MPa, and is 129.83 ± 12.59 , 166.72 ± 12.84 and 110.55 ± 10.76 MPa for the HA-1M-1S composite.
8. The increase in the mechanical properties of the HA-1M composite with the addition of the SiO₂ at an amount of 0.5 wt. % was related to the inhibition of the grain growth and the elimination of the microcracking.
9. It was determined that the in vitro bioactivity of the HA-1M composite could be increased with the addition of 0.5 % SiO₂.

REFERENCES

1. Angioni D., Orrù R., Cao G., Garroni S., Bellucci D., Cannillo V. (2023): Bioactivity enhancement by a ball milling treatment in novel bioactive glass-hydroxyapatite composites produced by spark plasma sintering. *Journal of the European Ceramic Society*, 43, 1220-1229. doi:10.1016/j.jeurceramsoc.2022.10.077
2. Sahmani S., Saber-Samandari S., Khandan A., Aghdam M.M. (2019): Influence of MgO nano particles on the mechanical properties of coated hydroxyapatite nanocomposite scaffolds produced via space holder technique: Fabrication, characterization and simulation. *Journal of the Mechanical Behavior of Biomedical Materials*, 95, 76-88. doi:10.1016/j.jmbbm.2019.03.014
3. Zhang X., Yin H., Xiao L., Li Z., Ma C., Xu W., Wang Y. (2022): Chitosan regulated electrochemistry for dense hydroxyapatite/MgO nanocomposite coating with antibiosis and osteogenesis on titanium alloy. *Colloid and Interface Science Communications*, 48, 100616. doi:10.1016/j.colcom.2022.100616
4. Boutinguiza M., Pou J., Comesaña R., Lusquiños F., de Carlos A., León B. (2012): Biological hydroxyapatite obtained from fish bones. *Materials Science and Engineering C*, 32, 478-486. doi:10.1016/j.msec.2011.11.021
5. Brzezińska-Miecznik J., Haberko K., Sitarz M., Bućko M.M., Macherzyńska B., Lach R. (2016): Natural and Synthetic hydroxyapatite/zirconia composites: A comparative study. *Ceramics International*, 42, 11126-11135. doi:10.1016/j.ceramint.2016.04.019
6. Muralithran G., Ramesh S. (2000): The effects of sintering temperature on the properties of hydroxyapatite. *Ceramics International*, 26, 221-230. doi:10.1016/S0272-8842(99)00046-2
7. Nasker P., Samanta A., Rudra S., Sinha A., Mukhopadhyay A.K., Das M. (2019): Effect of fluorine substitution on sintering behaviour, mechanical and bioactivity of hydroxyapatite. *Journal of the Mechanical Behavior of Biomedical Materials*, 95, 136-142. doi:10.1016/j.jmbbm.2019.03.032
8. Mardziah C.M., Ramesh S., Chandran H., Sidhu A., Krishnasamy S. (2023): Properties of sintered zinc hydroxyapatite bioceramic prepared using waste chicken eggshells as calcium precursor. *Ceramics International*, 49,12381-12389. doi:10.1016/j.ceramint.2022.12.098
9. Bazin T., Magnaudeix A., Mayet R., Carles P., Julien I., Demourgues A., Gaudon M., Champion E. (2021): Sintering and biocompatibility of copper-doped hydroxyapatite bioceramics. *Ceramics International*, 47, 13644-13654. doi:10.1016/j.ceramint.2021.01.225
10. Obada D.O., Salami K.A., Oyediji A.N., Fasanya O.O., Suleiman M.U., Ibisola B.A., Atta A.Y., Dodoo-Arhin D., Kuburi L.S., Dauda M., Dauda E.T. (2021): Solution combustion synthesis of strontium-doped hydroxyapatite: Effect of sintering and low compaction pressure on the mechanical properties and physiological stability. *Materials Letters*, 304, 130613. doi:10.1016/j.matlet.2021.130613
11. Landi E., Guizzardi S., Papa E., Galli C. (2021): Mg,Sr-Cosubstituted hydroxyapatite with improved structural properties. *Applied Sciences*, 11, 4930. doi:10.3390/app11114930
12. Cacciotti I., Bianco A., Lombardi M., Montanaro L. (2009): Mg-substituted hydroxyapatite nanopowders: Synthesis, thermal stability and sintering behaviour. *Journal of the European Ceramic Society*, 29, 2969-2978. doi:10.1016/j.jeurceramsoc.2009.04.038
13. Shamami D.Z., Rabie S.M., Shakeri M. (2022): Characterization of magnesium-hydroxyapatite functionally graded composites prepared by rapid microwave sintering technique. *Ceramics International*, 48, 12641-12653. doi:10.1016/j.ceramint.2022.01.133
14. Mihailescu N., Stan G.E., Duta L., Chifiriuc M.C., Bleotu C., Sopronyi M., Luculescu C., Otkar F.N., Mihailescu I.N. (2016): Structural, compositional, mechanical characterization and biological Assessment of bovine-derived hydroxyapatite coatings reinforced with MgF₂ or MgO for implants functionalization. *Materials Science and Engineering C*, 59, 863-874. doi:10.1016/j.msec.2015.10.078
15. Kumar S., Gautam C., Chauhan B.S., Srikrishna S., Yadav R.S., Rai S.B. (2020): Enhanced mechanical properties and hydrophilic behavior of magnesium oxide added hydroxyapatite nanocomposite: A bone substitute material for load bearing applications. *Ceramics International*, 46, 16235-16248. doi:10.1016/j.ceramint.2020.03.180
16. Kumar Y.N., Venkateswarlu B., Raju L.R., Dumpala R., Sunil B.R. (2021): Developing Zn-MgO composites for degradable implant applications by powder metallurgy route. *Materials Letters*, 302, 130433. doi:10.1016/j.matlet.2021.130433
17. Shaly A.A., Priya G.H., Mahendiran M., Linet J.M. (2022): A behavioural study of hydrothermally derived novel alumina/magnesia/hydroxyapatite (Al₂O₃/MgO/HA) bioceramic nanocomposite. *Journal of the Mechanical Behavior of Biomedical Materials*, 133, 105313.

- doi:10.1016/j.jmbbm.2022.105313
18. Katundi D., Bayraktar E., Gatamorta F., Miskioglu I. (2019): Design of Hydroxyapatite/Magnetite (HAP/Fe₃O₄) Based Composites Reinforced with ZnO and MgO for biomedical applications. *Biomedical Journal of Scientific & Technical Research*, 21(4), 16113-16121. doi:10.26717/BJSTR.2019.21.003649
 19. Demirkol N., Meydanoglu O., Gokce H., Oktar F.N., Kayali E.S. (2012): Comparison of Mechanical Properties of Sheep Hydroxyapatite (SHA) and Commercial Synthetic Hydroxyapatite (CSHA)-MgO Composites. *Key Engineering Materials*, 493-494, 588-593. doi:10.4028/www.scientific.net/KEM.493-494.588
 20. Oktar F.N., Agathopoulos S., Ozyegin L.S., Gunduz O., Demirkol N., Bozkurt Y., Salman S. (2007): Mechanical properties of bovine hydroxyapatite (BHA) composites doped with SiO₂, MgO, Al₂O₃, and ZrO₂. *Journal of Materials Science: Materials in Medicine*, 18, 2137-2143. doi:10.1007/s10856-007-3200-9
 21. Tan C.Y., Yaghoubi A., Ramesh S., Adzila S., Purbolaksono J., Hassan M.A., Kutty M.G. (2013): Sintering and mechanical properties of MgO-doped nanocrystalline hydroxyapatite. *Ceramics International*, 39, 8979-8983. doi:10.1016/j.ceramint.2013.04.098
 22. Evis Z., Usta M., Kutbay I. (2008): Hydroxyapatite and zirconia composites: Effect of MgO and MgF₂ on the stability of phases and sinterability. *Materials Chemistry and Physics*, 110, 68-75. doi:10.1016/j.matchemphys.2008.01.009
 23. Bodhak S., Bose S., Bandyopadhyay A. (2011): Influence of MgO, SrO, and ZnO dopants on electrothermal polarization behavior and in-vitro biological properties of hydroxyapatite ceramics. *Journal of the American Ceramic Society*, 94(4), 1281-1288. doi:10.1111/j.1551-2916.2010.04228.x
 24. Demirkol N. (2017): Bioactivity properties and characterization of commercial synthetic hydroxyapatite - 5 wt. % niobium oxide - 5 wt. % magnesium oxide composite. *Acta Physica Polonica A*, 132(3), 786-788. doi:10.12693/aphyspola.132.786
 25. Pazarlioglu S., Algan O., Isikogullari A.M., Gokce H. (2021): The effect of lanthanum addition on the microstructure and mechanical properties of Mg-modified hydroxyapatite ceramics. *Processing and Application of Ceramics*, 15[3], 226-237. doi:10.2298/PAC2103226P
 26. Bose S., Tarafder S., Banerjee S.S., Davies N.M., Bandyopadhyay A. (2011): Understanding in vivo response and mechanical property variation in MgO, SrO and SiO₂ doped β -TCP. *Bone*, 48, 1282-1290. doi:10.1016/j.bone.2011.03.685
 27. Mohamed K.R., Beherei H.H., Bassyouni G.T.E., Mahallawy N.E. (2013): Fabrication and mechanical evaluation of hydroxyapatite/oxide nano-composite materials. *Materials Science and Engineering C*, 33, 4126-4132. doi:10.1016/j.msec.2013.05.059
 28. Moreno-Pereza B., Matamoros-Veloza Z., Rendon-Angeles J.C., Yanagisawa K., Onda A., Pérez-Terrazas J.E., Mejia-Martínez E.E., Díaz O.B., Rodríguez-Reyes M. (2020): Synthesis of silicon-substituted hydroxyapatite using hydrothermal process. *Boletín De La Sociedad Española De Cerámica Y Vidrio*, 59, 50-64. doi:10.1016/j.bsecv.2019.07.001
 29. Porter A.E., Best S.M., Bonfield W. (2003): Ultrastructural comparison of hydroxyapatite and silicon substituted hydroxyapatite for biomedical applications. *Journal of Biomedical Materials Research Part A*, 68, 133-141. doi:10.1002/jbm.a.20064
 30. Asmi D., Sulaiman A., Oktavia I.L., Badaruddin M., Zulfia A. (2016): Synthesis and characterisation of composite based biohydroxyapatite bovine bone mandible waste (BHAp) doped with 10 wt. % amorphous SiO₂ from rice husk by solid state reaction. *American Institute of Physics*, 1725, 020009-7. doi:10.1063/1.4945463
 31. Nakahira A., Nakata K., Numako C., Murata H., Matsunag K. (2011): Synthesis and evaluation of calcium-deficient hydroxyapatite with SiO₂. *Materials Sciences and Applications*, 2, 1194-1198. doi:10.4236/msa.2011.29161
 32. Kivitz E., Görke R., Schilling A.F., Zhang J., Heinrich J.G. Influence of processing parameters on microstructure and biocompatibility of surface laser sintered hydroxyapatite-SiO₂ composites. *Journal of Biomedical Materials Research Part A*, 101B, 568-575. doi:10.1002/jbm.b.32858
 33. Padovini D.S.S., Azevedo-Silva L.J., Ferrairo B.M., Pereira L.F., Minim P.R., Pontes F.M.L., Fortulan C.A., Borges A.F.S. (2023): Hydroxyapatite/ZrO₂@SiO₂ bioceramic composite: Producing a promising biomaterial from natural sources. *MRS Communications*, doi:10.1557/s43579-023-00408-4
 34. Pazarlioglu S., Salman S. (2017): Sintering effect on the microstructural, mechanical, and in vitro bioactivity properties of a commercially synthetic hydroxyapatite. *Journal of the Australian Ceramic Society*, 53, 391-401. doi:10.1007/s41779-017-0048-4
 35. Lim G.K., Wang J., Ng S.C., Chew C.H., Gan L.M. (1997): Processing of hydroxyapatite via microemulsion and emulsion routes. *Biomaterials*, 18[21], 1433-1439. doi:10.1016/S0142-9612(97)00081-1
 36. Mohammed G., El-Gamal S. (2021): The role of MgO nanoparticles addition, and γ -irradiation on the microstructural, and tensile properties of Al-1100 alloy. *Journal of Composite Materials*, 55(16), 2135-2149. doi:10.1177/0021998320983411
 37. ZiJue Z., Yi F., Hao Z., Gang Q., Jing-Cheng Z., XueBin Z., XiaoChen H. (2021): Effects of different atmospheres on the arc erosion behaviors of Ti₃SiC₂ cathodes. *Science China Technological Science*, 64, 620-628. doi:10.1007/s11431-019-1552-x
 38. Pandey A., Nigam V.K., Balani K. (2018): Multi-length scale tribology of hydroxyapatite reinforced with ceria and silver. *Wear*, 404-405, 12-21. doi: 10.1016/j.wear.2018.01.006
 39. Yemisci I., Mutlu O., Gulsoy N., Kunal K., Atrec S., Gulsoy H.O. (2019): Experimentation and analysis of powder injection molded Ti₁₀Nb₁₀Zr alloy: a promising candidate for electrochemical and biomedical application. *Journal of Materials Research and Technology*, 8[6], 5233-5245. doi: 10.1016/j.jmrt.2019.08.046
 40. Wang P.E., Chaki T.K. (1993): Sintering behaviour and mechanical properties of hydroxyapatite and dicalcium phosphate. *Journal of Materials Science: Materials in Medicine*, 4, 150-158. doi:10.1007/BF00120384
 41. Terpstra R.A., Driesse F.C.M. (1984): The CaO-MgO-P₂O₅ system at 1000°C for P₂O₅ < 33.3 mol. %. *Zeitschrift für anorganische und allgemeine Chemie*, 515[8], 213-224. doi:10.1002/zaac.19845150
 42. Cao J., Lian R., Jiang X. (2020): Magnesium and fluoride doped hydroxyapatite coatings grown by

- pulsed laser deposition for promoting titanium implant cytocompatibility. *Applied Surface Science*, 515[15], 146069 doi:10.1016/j.apsusc.2020.146069
43. Stipnice L., Salma-Ancane K., Jakovlevs D., Borodajenko N., Berzina-Cimdina L. (2013): The study of magnesium substitution effect on physicochemical properties of hydroxyapatite. *Material Science and Applied Chemistry*, 28, 51-57. doi:10.7250/msac.2013.009
 44. Noviyanti A.R., Rahayu I., Fauzia R.P., Risdiana. (2021): The effect of Mg concentration to mechanical strength of hydroxyapatite derived from eggshell. *Arabian Journal of Chemistry*, 14[4], 103032. doi:10.1016/j.arabjc.2021.103032
 45. Enderle R., Gotz-Neunhoeffler F., Gobbels M., Muller F.A., Grei P. (2005): Influence of magnesium doping on the phase transformation temperature of β -TCP ceramics examined by Rietveld refinement. *Biomaterials*, 26[17], 3379-3384. doi:10.1016/j.biomaterials.2004.09.017
 46. Gozalian A., Behnamghader A., Daliri M., Moshkforoush A. (2011): Synthesis and thermal behavior of Mg-doped calcium phosphate nano powders via the sol-gel method. *Scientia Iranica, Transactions F: Nanotechnology*, 18[6], 1614-1622. doi:10.1016/j.scient.2011.11.014
 47. Cheng H., Chabok R., Guan X., Chawla A., Li Y., Khademhosseini A., Jang H.L. (2018): Synergistic inter play between the two major bone minerals, hydroxyapatite and whitlockite nanoparticles, for osteogenic differentiation of mesenchymal stem cells. *Acta Biomaterialia*, 69[15], 342-351. doi:10.1016/j.actbio.2018.01.016
 48. Htun M.M., Noor A.F.M., Kawashita M., Ismail Y.M.B. (2020): Characterization and evaluation of copper-doped akermanite ceramic. *IOP Conference Series: Materials Science and Engineering*, 943, 012008. doi:10.1088/1757-899X/943/1/012008
 49. Chen X., Liao X., Huang Z., You P., Chen C., Kang Y., Yin G. (2010): Synthesis and characterization of novel multiphase bioactive glass-ceramics in the CaO-MgO-SiO₂ system. *Journal of Biomedical Materials Research Part B: Applied Biomaterials*, 93[1], 194-202. doi:10.1002/jbm.b.31574
 50. Tulyaganov D.U., Agathopoulos S., Ventura J.M., Karakassides M.A., Fabrichnaya O., Ferreira J.M.F. (2006): Synthesis of glass-ceramics in the CaO-MgO-SiO₂ system with B₂O₃, P₂O₅, Na₂O and CaF₂ additives. *Journal of the European Ceramic Society*, 26[8], 1463-1471. doi:10.1016/j.jeurceramsoc.2005.02.009
 51. Sepp B., Kunzmann T. (2001): The stability of clinopyroxene in the system CaO-MgO-SiO₂-TiO₂ (CMST). *American Mineralogist*, 86[3], 265-270. doi:10.2138/am-2001-2-308
 52. Tribaudino M., Nestola F., Meneghini C., Bromiley G.D. (2003): The high-temperature P2_{1/c}-C2_{1/c} phase transition in Fe-free Ca-rich P2_{1/c} clinopyroxenes, *Physics and Chemistry of Minerals*, 30, 527-535. doi:10.1007/s00269-003-0338-y
 53. Rasskazova L.A., Zhuk I.V., Korotchenko N.M., Brichkov A.S., Chen Y.W., Paukshtis E.A., Ivanov V.K., Kurzina I.A., Kozik V.V. (2019): Synthesis of magnesium- and silicon-modified hydroxyapatites by microwave-assisted method. *Science Reports*, 9, 14836. doi:10.1038/s41598-019-50777-x
 54. Abbasi-Shahni M., Hesaraki S., Behnam-Ghader A.A., Hafezi-Ardakani M. (2012): Mechanical properties and in vitro bioactivity of β -tricalcium phosphate, merwinite nanocomposites. *Key Engineering Materials*, 493-494, 582-587. doi:10.4028/www.scientific.net/KEM.493-494.582
 55. Osborn E.F. (1943): The compound merwinite (3CaO.MgO.2SiO₂) and its stability relations within the system CaO-MgO-SiO₂. *The Journal of the American Ceramic Society*, 26(10), 321-332. doi:10.1111/j.1151-2916.1943.tb14452.x
 56. Liao J., Qing G., Zhao B. (2023): Phase equilibria studies in the CaO-MgO-Al₂O₃-SiO₂ system with Al₂O₃/SiO₂ weight ratio of 0.4. *Metals*, 13, 224. doi:10.3390/met13020224
 57. Sahu I.P., Bisen D.P., Murthy K.V.R., Tamrakar R.K. (2017): Studies on the luminescence properties of cerium co-doping on Ca₂MgSi₂O₇:Eu²⁺ phosphor by solid-state reaction method. *Luminescence*, 32, 1263-1276. doi:10.1002/bio.3320
 58. Li J., Xu A., He D., Yang Q., Tian N. (2013): Effect of FeO on the formation of spinel phases and chromium distribution in the CaO-SiO₂-MgO-Al₂O₃-Cr₂O₃ system. *International Journal of Minerals, Metallurgy and Materials*, 20[3], 253-259. Doi:10.1007/s12613-013-0720-9
 59. Tulyaganov D.U., Dimitriadis K., Agathopoulos S., Fernandes H.R. (2023): Glasses and glass-ceramics in the CaO-MgO-SiO₂ system: Diopside containing compositions - A brief review. *Journal of Non-Crystalline Solids*, 612, 122351. doi:10.1016/j.jnoncrysol.2023.122351
 60. Almuhamadi J., Karpukhina N., Cattell M. (2014): Diopside glass-ceramics for dental and biomedical applications. *Advances in Science and Technology*, 96, 15-20. doi:10.4028/www.scientific.net/AST.96.15
 61. Yamagata C., Leme D.R., Rodrigues V.G., Eretides G.T., Rodas A.C.D. (2022): Three routes for the synthesis of the bioceramic powder of the CaO-MgO-SiO₂ system. *Ceramics International*, 48[7], 9681-9691. doi:10.1016/j.ceramint.2021.12.169
 62. Pandolfo F., Cámara F., Domeneghetti M.C., Alvaro M., Nestola F., Karato S.I., Amulele G. (2015): Volume thermal expansion along the jadeite-diopside join. *Physics and Chemistry of Minerals*, 42, 1-14. doi:10.1007/s00269-014-0694-9
 63. Ślósarczyk A., Klisch M., Błażewicz M., Piekarczyk J., Stobierski L., Rapacz-Kmita, A. (2000): Hot pressed hydroxyapatite-carbon fibre composites. *Journal of the European Ceramic Society*, 20[9], 1397-1402. doi:10.1016/S0955-2219(00)00014-5
 64. García-Páez I.H., Pena P., Baudin C., Rodríguez M.A., Córdoba E., Aza Antonio H.D. (2016): Processing and in vitro bioactivity of β -Ca₃(PO₄)₂-CaMg(SiO₃)₂ ceramic with the eutectic composition. *Boletín De La Sociedad Española De Cerámica Y Vidrio*, 55[1], 1-12. doi:10.1016/j.bsecv.2015.10.004
 65. Feng P., Gao C., Shuai C., Peng S. (2015): Toughening and strengthening mechanisms of porous akermanite scaffolds reinforced with nano-titania. *RSC Advances*. 5[5], 3498-3507. doi:10.1039/C4RA12095G
 66. Shen C., Zhang S., Cao W., Cong H., Yu H., Wang J., Zhang H. (2015): Thermal and electromechanical properties of melilite-type piezoelectric single crystals. *Journal of Applied Physics*, 117, 064106. doi: 10.1063/1.4908113
 67. Xiuhua G., Kexing S., Shuhua L., Cuihua Z. (2012): Thermal expansion behavior of MgO/Cu composite with lower MgO volume fractions. *Materials Research Bulletin*, 47[11], 3211-3215. doi:10.1016/j.materresbull.2012.08.012
 68. Wyllie P.J., Huang W.L. (1975): Peridotite, kimberlite,

- and carbonatite explained in the system CaO-MgO-SiO₂-CO₂. *Geology*, 3[11], 621-624. doi:10.1130/0091-7613(1975)3<621:PKACEI>2.0.CO;2
69. Biggar G.M., O'hara M.J. (1970): Melting of forsterite, monticellite, merwinite, spinel, and periclase assemblages. *Journal of The American Ceramic Society*, 53[10], 534-537. doi:10.1111/j.1151-2916.1970.tb15959.x
 70. Kaminskii A.A., Bohati L., Eichler H.J., Lux O., Rhee H., Burianek M., Becker P. (2020): Stimulated raman scattering in melilite-type crystals Ca₂MgSi₂O₇ and Ca₂Ga₂SiO₇. *Crystal Research and Technology*, 2000038, 1-12. doi:10.1002/crat.202000038
 71. Davis B.T.C., Boyd F.R. (1996): The join Mg₂SiO₆-CaMgSi₂O₆ at 30 kilobars pressure and its application to pyroxenes from kirnberlites. *Journal of Geophysical Research*, 71[4], 3567-3576. doi:10.1029/JZ0711014P03567
 72. Mohammedi H., Hei B.Z., Ismail Y.M.B., Shariff K.A., Noor A.F.M. (2020): Green synthesis of calcium magnesium silicate (CMS-Akermanite) using natural biowastes by solid-state sintering route. *Malaysian Journal of Microscopy*, 16[2], 66-76. doi:10.1039/D2NJ05066H
 73. Wang H., Li D., Yang Q., Lei R., Ma H., Xu S. (2014): Sintering behavior and dielectric properties of Al₂O₃ ceramics with CaMgSi₂O₆ addition. *Materials Research Bulletin*, 54, 66-72. doi:10.1016/j.materresbull.2014.03.014
 74. Bindi L., Bonazzi P., Dušek M., Petříček V., Chapuis G. (2001): Five-dimensional structure refinement of natural melilite, (Ca_{1.89}Sr_{0.01}Na_{0.08}K_{0.02})(Mg_{0.92}Al_{0.08})(Si_{1.98}Al_{0.02})O₇. *Acta Crystallographica*, B57, 739-746. doi:10.1107/S0108768101014495
 75. Araki T. Moore P.B. (1972): Atomic arrangement of merwinite, Ca₃Mg[SiO₄]₂, An unusual dense-packed structure of geophysical interest. *American Mineralogist*, 57, 1355-1374.
 76. Tseng Y.S., Su Y.H., Chen C.L., Zhang J., Wang C.K., Hanaor D.A.H., Chen W.F. (2023): Bioceramics in the CaMgSi₂O₆-Li₂O system: A glass-ceramic strategy for excellent mechanical strength and enhanced bioactivity by spontaneous elemental redistribution. *Advanced Materials Interfaces*, 10, 2202491. doi:10.1002/admi.202202491
 77. Calvo C., Gopal R. (1975): The crystal structure of whitlockite from the Palermo quarry. *American Mineralogist*, 60[1-2], 120-133.
 78. Ringdalen E., Tangstad M. (2016): Softening and melting of SiO₂, an important parameter for reactions with quartz in Si Production. *Advances in Molten Slags, Fluxes, and Salts: Proceedings of the 10th International Conference on Molten Slags, Fluxes and Salts*, doi:10.1007/978-3-319-48769-4_4
 79. Ronchi C., Sheindlin M. (2001): Melting point of MgO. *Journal of Applied Physics*, 90[7], 3325-3331. doi:10.1063/1.1398069
 80. Kim S.R., Lee J.H., Kim Y.T., Riu D.H., Jung S.J., Lee Y.J., Chung S.C., Kim Y.H. (2003): Synthesis of Si, Mg substituted hydroxyapatites and their sintering behaviors. *Biomaterials*, 24[8], 1389-1398. doi:10.1016/S0142-9612(02)00523-9
 81. Ke D., Robertson S.F., Dernell W.S., Bandyopadhyay A., Bose S. (2017): Effects of MgO and SiO₂ on plasma-sprayed hydroxyapatite coating: An in vivo study in rat distal femoral defects. *ACS Applied Materials and Interfaces*, 9[31], 25731-25737. doi:10.1021/acsami.7b05574
 82. Filho C.R.S., de Souza Carvalho F.M., Guedes-Silva C.C. (2022): Mechanical properties and in vitro bioactivity of silicon nitride ceramics with SiO₂, CaO, and MgO additions. *Journal of Biomedical Materials Research, Part B Applied Biomaterials*, 110, 507-516. doi:10.1002/jbm.b.34930
 83. Silva V.V., Domingues R.Z., Lameiras F.S. (2001): Microstructural and mechanical study of zirconia-hydroxyapatite (ZH) composite ceramics for biomedical applications. *Composite Science and Technology*, 61[2], 301-310. doi:10.1016/S0266-3538(00)00222-0
 84. Bulut B., Erkmen Z.E., Kayali E.S. (2016): Biocompatibility of hydroxyapatite-alumina and hydroxyapatite-zirconia composites including commercial inert glass (CIG) as a ternary component. *Journal of Ceramic Science and Technology*, 07 [03], 263-276. doi: 10.4416/JCST2016-00011
 85. Pazarlioglu S., Salman S. (2019): Effect of yttria on thermal stability, mechanical and in vitro bioactivity properties of hydroxyapatite/alumina composite. *Journal of Ceramic Processing Research*, 20[1], 99-112. doi:10.36410/jcpr.2019.20.1.99
 86. Lazar D.R.R., Cunha S.M., Ussui V., Fancio E., de Lima N.B., Bressiani, A.H.A. (2008): Influence of synthesis route on phase formation and sinterability of hydroxyapatite-zirconia composites. *Materials Science Forum*, 591-593, 722-727. doi:10.4028/www.scientific.net/MSF.591-593.722
 87. Lopes M.A., Monteiro F.J., Santos J.D. (1999): Glass-reinforced hydroxyapatite composites: Secondary phase proportions and densification effects on biaxial bending strength. *Journal of Biomedical Materials Research*, 48[5], 734-740. doi:10.1002/(sici)1097-4636(1999)48:5
 88. Bellucci D., Sola A., Cannillo V. (2016): Hydroxyapatite and tricalcium phosphate composites with bioactive glass as second phase: State of the art and current applications. *Journal of Biomedical Materials Research A*, 104A[4], 1030-1056. doi:10.1002/jbm.a.35619
 89. Curran D.J., Fleming T.J., Towler M.R., Hampshire S. (2011): Mechanical parameters of strontium doped hydroxyapatite sintered using microwave and conventional methods. *Journal of The Mechanical Behavior of Biomedical Materials*, 4[8], 2063-2073. doi:10.1016/j.jmbbm.2011.07.005
 90. Xu J.L., Khor K.A. (2007): Chemical analysis of silica doped hydroxyapatite biomaterials consolidated by a spark plasma sintering method. *Journal of Inorganic Biochemistry*, 101[2], 187-195. doi:10.1016/j.jinorgbio.2006.09.030
 91. Tolouei R., Ramesh S., Tan C.Y., Amiryan M., Teng W.D. (2011): Effect of grain size on vickers microhardness and fracture toughness in calcium phosphate bioceramics. *Applied Mechanics and Materials*, 83, 237-243. doi:10.4028/www.scientific.net/AMM.83.237
 92. Gu Y.W., Loh N.H., Khor K.A., Tor S.B., Cheang P. (2002): Spark plasma sintering of hydroxyapatite powders. *Biomaterials*, 23[1], 37-43. doi:10.1016/S0142-9612(01)00076-X
 93. Hu X., Zhang W., Hou D. (2020): Synthesis, microstructures and mechanical properties of tricalcium phosphate-hydroxyapatite (TCP/HA) composite ceramic. *Ceramics International*, 46[7], 9810-9816. doi:10.1016/j.ceramint.2019.12.254
 94. Kobayashi S., Murakoshi T. (2014): Characterization of mechanical properties and bioactivity of hydroxyapatite/ β -tricalcium phosphate composites. *Advanced Composite*

- Materials*, 23[2], 163-177. doi:10.1080/09243046.2013.844897
95. Wu C., Chang J. (2006): A novel akermanite bioceramic: Preparation and characteristics. *Journal of Biomaterials Applications*, 21[2], 119-129. doi:10.1177/08853282060579
96. Nadernezhad A., Moztarzadeh F., Hafezi M., Barzegar-Bafrooei H. (2014): Two step sintering of a novel calcium magnesium silicate bioceramic: Sintering parameters and mechanical characterization. *Journal of the European Ceramic Society*, 34[15], 4001-4009. doi:10.1016/j.jeurceramsoc.2014.05.014
97. Byeongguk K., Seunggu K. (2020): Crystal growth behavior, nanometer microstructure, and mechanical properties of diopside-based glass-ceramics. *Journal of Nanoscience and Nanotechnology*, 20[1], 183-189. doi:10.1166/jnn.2020.17290.
98. Bhattacharjee A., Hassan R., Gupta A., Verma M., Murugan P.A., Sengupta P., Saravanan M., Manna I., Balani K. (2020): Effect of Zn and Co doping on antibacterial efficacy and cytocompatibility of spark plasma sintered hydroxyapatite. *Journal of the American Ceramic Society*, 103, 4090-4100. doi:10.1111/jace.17077
99. Shaly A.A., Priya G.H., Mahendiran M., Linet J.M., Mani J.A.M. (2022): An intrinsic analysis on the nature of alumina (Al₂O₃) reinforced hydroxyapatite nanocomposite. *Physica B: Condensed Matter*, 642, 414100. doi:10.1016/j.physb.2022.414100
100. Shen H.Z., Guo N., Zhao L., Shen P. (2020): Role of ion substitution and lattice water in the densification of cold-sintered hydroxyapatite. *Scripta Materialia*, 177, 141-145. doi:10.1016/j.scriptamat.2019.10.024
101. Bose S., Dasgupta S., Tarafder S., Bandyopadhyay A. (2010): Microwave processed nanocrystalline hydroxyapatite: Simultaneous enhancement of mechanical and biological properties. *Acta Biomaterialia*, 6[9], 3782-3790. doi: 10.1016/j.actbio.2010.03.016
102. Hoepfner T.P., Case E.D. (2004): An estimate of the critical grain size for microcracks induced in hydroxyapatite by thermal expansion anisotropy. *Materials Letters*, 58[3-4], 489-492. doi:10.1016/S0167-577X(03)00531-7
103. Halouani R., Bernache-Assolant D., Champion E., Ababou A. (1994): Microstructure and related mechanical properties of hot pressed hydroxyapatite ceramics. *Journal of Materials Science: Materials In Medicine*, 5, 563-568. doi:10.1007/BF00124890
104. Ji C., He B., Yun S., Bai X., Lin B. (2023): The fracture mechanical behavior simulation of calcium-deficient hydroxyapatite crystals by molecular dynamics and first-principles calculation. *Journal of the Mechanical Behavior of Biomedical Materials*, 137, 105526. doi:10.1016/j.jmbbm.2022.105526
105. Chen B., Zhang T., Zhang J., Lin Q., Jiang D. (2008): Microstructure and mechanical properties of hydroxyapatite obtained by gel-casting process. *Ceramics International*, 34[2], 359-364. doi:10.1016/j.ceramint.2006.10.021
106. Sharafabadi A.K., Abdellahi M., Kazemi A., Khandan A., Ozada N. (2017): A novel and economical route for synthesizing akermanite (Ca₂MgSi₂O₇) nano-bioceramic. *Materials Science and Engineering C*, 71, 1072-1078. doi:10.1016/j.msec.2016.11.021
107. Ku J.K., Kim I., Shim J.H., Kim Y.H., Kim B.H., Kim Y.K., Yun P.Y. (2022): The effect of whitlockite as an osteoconductive synthetic bone substitute material in animal bony defect model. *Materials*, 15, 1921. doi:10.3390/ma15051921
108. Dasgupta S., Tarafder S., Bandyopadhyay A., Bose S. (2013): Effect of grain size on mechanical, surface and biological properties of microwave sintered hydroxyapatite. *Materials Science and Engineering C*, 33, 2846-2854. doi:10.1016/j.msec.2013.03.004
109. Rezapourian M., Kamboj N., Jasiuk I., Hussainova I. (2022): Biomimetic design of implants for long bone critical-sized defects. *Journal of the Mechanical Behavior of Biomedical Materials*, Volume 134, 105370. doi:10.1016/j.jmbbm.2022.105370
110. Ruiz-Aguilar C., Alcántara-Quintana L.E., Aguilar-Reyes E.A., Olivares-Pinto U. (2022): Fabrication, characterization, and in vitro evaluation of β-TCP/ZrO₂-phosphate-based bioactive glass scaffolds for bone repair. *Boletín de la Sociedad Española de Cerámica y Vidrio*, 61[3], 191-202. doi:10.1016/j.bsecv.2020.09.004
111. Salman S.M., Salama S.N., Abo-Mosallam H.A. (2011): Crystallization and ability of hydroxyapatite formation in some trivalent oxides containing Na-Ca-silicate glass-ceramics, *Silicon*, 3, 199-205. doi:10.1007/s12633-011-9099-2
112. Patel S., Samudrala R.K., Palakurthy S., Manavathi B., Gujjala R., Azeem A. (2022): In vitro evaluation and mechanical studies of MgO added borophosphate glasses for biomedical applications. *Ceramics International*, 48[9], 12625-12634. doi:10.1016/j.ceramint.2022.01.130
113. Kaur P., Singh K.J., Kaur R. (2022): In vitro analysis of SiO₂-MgO-P₂O₅-CaO bioactive material for bone regeneration applications. *Materials Today: Proceedings*, 68[4], 799-802. doi:10.1016/j.matpr.2022.06.155
114. Díaz-Pérez M., Grima L., Moshtaghioun B.M., Pena J.I., CaO-MgO-SiO₂-P₂O₅-based multiphase bio-ceramics fabricated by directional solidification: Microstructure features and in vitro bioactivity studies. *Ceramics International*, 47, 17041-17048. doi: 10.1016/j.ceramint.2021.03.011
115. Aurlybekulya A., Pogrebnjakb A.D., Sukhodub, L.F., Sukhodub, L.B., Kistaubayeva, A.S., Savitskaya, I.S., Shokatayeva, D.H., Bondar, O.V., Shaimardanova, Zh. K., Plotnikova, S.V., Shaimardanova, B.H., Digel, I. (2019): Synthesis, characterization, in vitro biocompatibility and antibacterial properties study of nanocomposite materials based on hydroxyapatite biphasic ZnO micro- and nanoparticles embedded in alginate matrix. *Materials Science and Engineering C*, 104, 1099. doi:10.1016/j.msec.2019.109965